NASW-4435

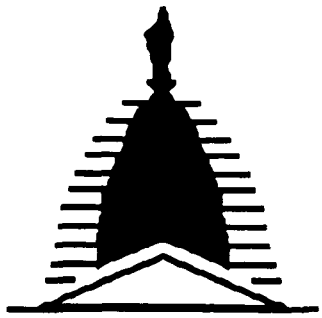

UNIVERSITY of
NOTRE DAME

NASA/USRA UNIVERSITY ADVANCED DESIGN PROGRAM 1990-1991

UNIVERSITY SPONSOR
BOEING COMMERCIAL AIRPLANE COMPANY

FINAL DESIGN PROPOSAL

KAPPA GROUP - THE INITAL GUESS

A Proposal in Response to a Commercial Air Transportation Study

May 1991

Department of Aerospace and Mechanical Engineering
University of Notre Dame
Notre Dame, IN 46556

Table of Contents

1. INTRODUCTION

1.1 Nomenclature

RWT	Real World Time
AWT	Aero World Time
RPV	Remotely Piloted Vehicle
Re	Reynolds Number
V	Velocity
Vmin	Minimum Velocity
Vmax	Maximum Velocity
Vstall	Stall Velocity
S	Wing Area
Vv	Vertical Volume Ratio
Vh	Horizontal Volume Ratio
b	Span
c	Chord
AR	Aspect Ratio
L	Taper Ratio
W	Sweep Angle
G	Dihedral Angle
Cdp	Drag Coefficient for Section "p"
Ap	Area on which Cdp is based
Cl	Section Lift Coefficient
Cd	Section Drag Coefficient
Cdo	Form Drag Coefficient
L	Lift
D	Drag
L/D	Lift to Drag Ratio
e	Efficiency
a	Angle of Attack
a_o	Lift Curve Slope
C.G.	Center of Gravity
i	Current
amp	Ampere
N.P.	Neutral Point
Cm	Moment Coefficient
Cn	Yaw Coefficient
Cl	Roll Coefficient
S.F.S.M.	Stick Fixed Static Margin
S.M.	Static Margin
d	Deflection Angle

1.2 Executive Summary

Kappa Aerospace presents their Aeroworld aircraft *"The Initial Guess."* This aircraft is designed to generate profit in the market which is currently controlled by the train and boat industry. The main priority of the design team was to develop an extremely efficient aircraft that could be sold at a reasonable price. *"The Initial Guess"* offers a quick and safe alternative to the existing means of transportation at a competitive price. The cruise velocity of 28 ft/sec. allows all flights to be between 20 and 45 minutes, which is a remarkable savings in time compared to travel by boat or train.

"The Initial Guess" is propelled by a single Astro-05 engine with a Zinger 10-6 propeller. The Astro-05 is not an extremely powerful engine, however it provides enough thrust to meet the design and safety requirements. The major advantage of the Astro-05 is that it is the most efficient engine available. The fuel efficiency of the Astro-05 is what puts the Kappa Aerospace aircraft ahead of the competition. The money saved on an efficient engine can be passed on as lower ticket prices or increased revenue.

"The Initial Guess" has a payload of 56 passengers and a wingspan of 7 ft. The 7 ft. wingspan allows the aircraft to fit into the gates of all of the cities that are targeted. Future endeavors of Kappa Aerospace will include fitting a stretch version of *"The Initial Guess"* with a larger propulsion system. This derivative aircraft will be able to carry more passengers and will be placed on the routes which have the greatest demand for travel.

The fuselage and empennage are made of a wooden truss configuration, while the wing is made of a rib/spare configuration. The stress carrying elements are made of spruce, the non-stress carrying elements are made of balsa. The wing is removable for easy access into the fuselage. The easy access to the batteries will keep maintenance costs down.

"The Initial Guess" will cost $246,000 to produce. The ticket price will be $75 flat fee and $12/50 ft. This ticket price will generate profit at the most expensive fuel price and assuming that the plane flies at capacity the production cost will be made back in 49 flights. *"The Initial Guess"* provides

an extremely rapid return on investment and will be competitive with the already existing modes of transportation.

1.3 Initial Concepts

To initiate the development of the design of the aircraft Kappa Aerospace sought to build, each member of the group submitted their own concept. Each of the preliminary designs were reviewed by the entire group so that the merits of each design could be fused into the preliminary group concept. Through review of each design, it was sought to utilize the various positive aspects of each concept to produce the best possible aircraft configuration for Kappa Aerospace. Representations of these initial concepts are shown in Figures 1-1 and 1-2.

Figure 1 - 1

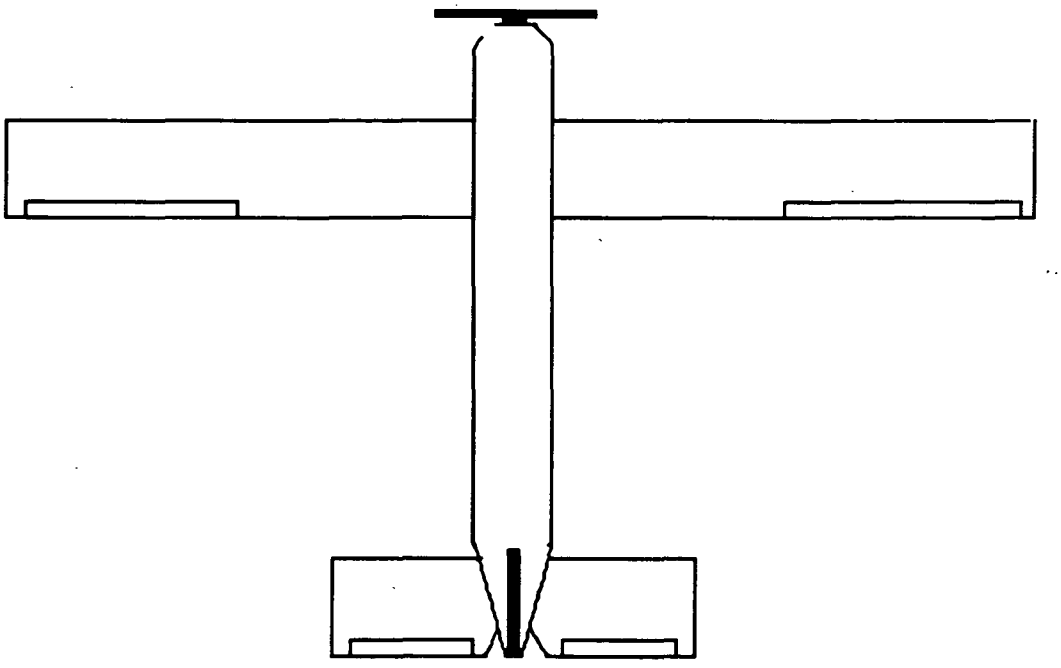

Both of these concepts embodied the general configuration of the aircraft decided upon by our group. This configuration includes the following: forward wing, rear vertical and horizontal tails, and a single prop engine. Aside from these general similarities, additional components from each of these designs were either incorporated into our group concept or were ruled

out in favor of concepts presented in other designs. From the concept proposed by Figure 1-1, the straight wing and square fuselage were retained. By incorporating these characteristics into our final design, we could minimize the complexity of the construction of the wing and fuselage to compensate for our lack of experience in construction. Not all aspects of this design were retained, though. It was decided to not incorporate the ailerons on the wings so as to reduce the number of servos needed for the aircraft and to simplify the construction of the wing. The design of Figure 1-2 made

Figure 1 - 2

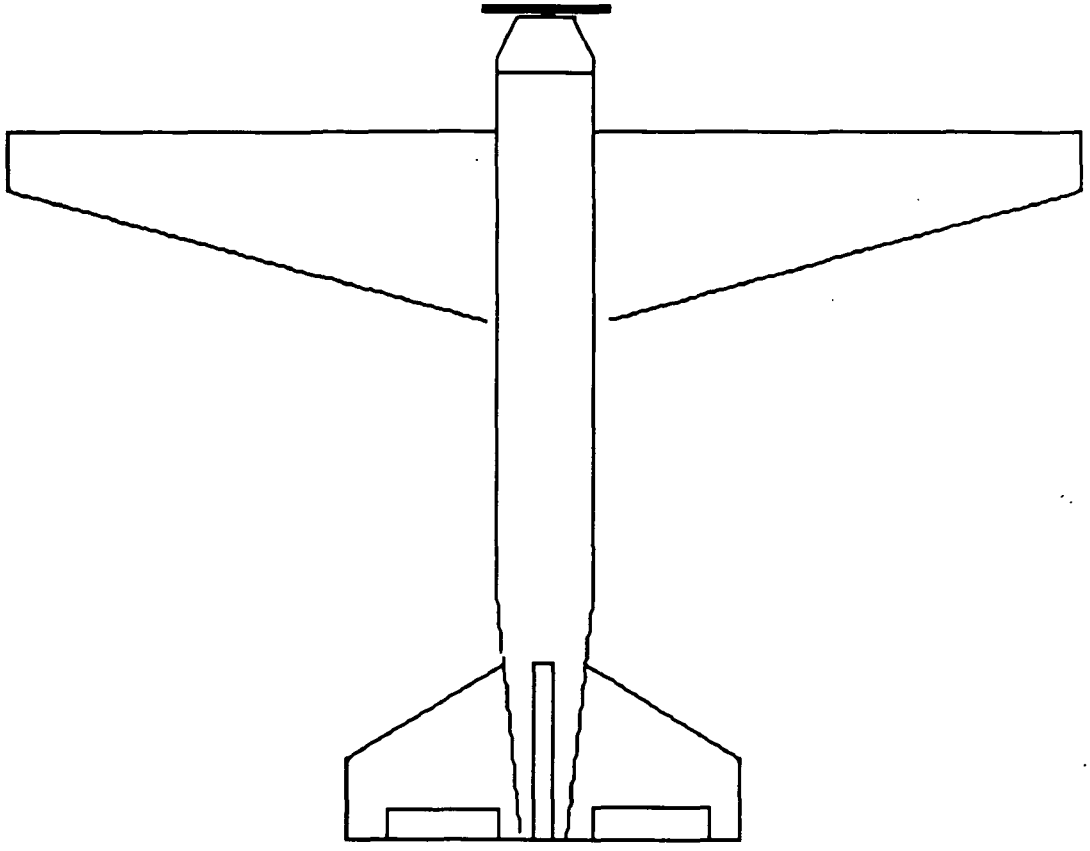

similar contributions to the final preliminary concept. For example, the large fuselage tapers of the nose and the tail were retained, the former to reduce blockage of the propeller's thrust and the latter to reduce the overall drag of the aircraft. Another characteristic obtained from this design is the use of dihedral for roll stability. (Not shown due to the overhead view of the

aircraft) The tapered wing of Figure 1-2 was rejected again for construction considerations.

Eventually we arrived at our final concept (Shown in Section 1.4) after thorough review of each members individual concept. The process of formulating an individual concept and evaluating other member's concepts aided in the combining of everyone's idea into an aircraft which each member of the group had a contribution. The contributions provided each member with confidence in the aircraft's ability to be manufactured and marketed for a profit.

Kappa Aerospace

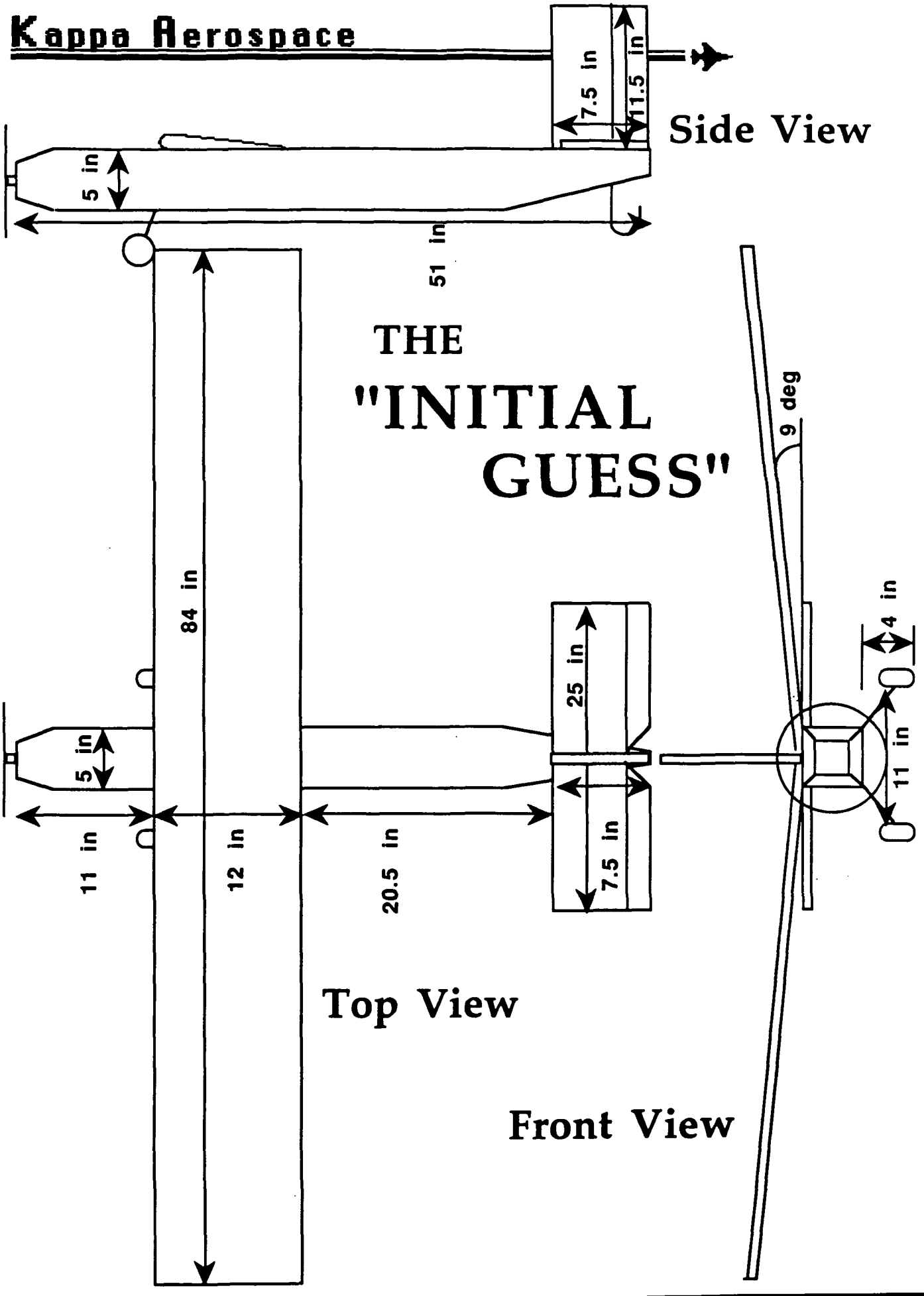

1.5 Design Specification Summary

Performance Specifications

V_{cruise}	28 ft/s
Turn radius	60 ft
Endurance	4 min
Range	5500 ft
Weight	61 oz.

Wing Characteristics

Area	1008 in^2
Span	84 in.
Chord	12 in.
Aspect Ratio	7
Taper Ratio	1
Sweep angle	0°
Dihedral	9°
Airfoil section	NACA 4415

Fuselage

Length	51 in.
Height	5 in.
Width	5 in.
Volume	550 in.

Empennage

Horiz tail area	187 $in.^2$
Horiz tail span	25 in.
Horiz tail chord	7.5 in.
Vert tail area	86.25 $in.^2$
Vert tail chord	7.5 in.
Airfoil section	Flat Plate

Aerodynamics

Clmax	1.05
Cdo	0.029
efficiency - e	0.71
Alpha stall	8°
L/D max	14.83
Alpha L/Dmax	0°

Propulsion

Type	Astro 05
Placement	Nose
Cruise current draw.	3.33 Amps
Propeller	Zinger 10-6

1.6 Mission Definition

The Kappa Aerospace aircraft is in response to the demand for improved transportation in Aeroworld. The existing means of transportation are trains and boats. Kappa Aerospace was asked to develop an aircraft that would be a successful business investment. The first step in answering the demand for an air carrier was to determine the ultimate goal for developing any type of aircraft designed by Kappa Aerospace: to produce a low cost, efficient aircraft that will generate profit.

The major economic design variables of Kappa Aerospace's aircraft were determined to be fuel cost, maintenance cost, and production cost. Of these three the fuel cost is the variable which was of the greatest concern during the design process. The major design variables of the aircraft included weight, passenger capacity, and range. In meeting these design variables Kappa Aerospace will be able to produce an aircraft that will generate substantial profit.

Figure 1-3

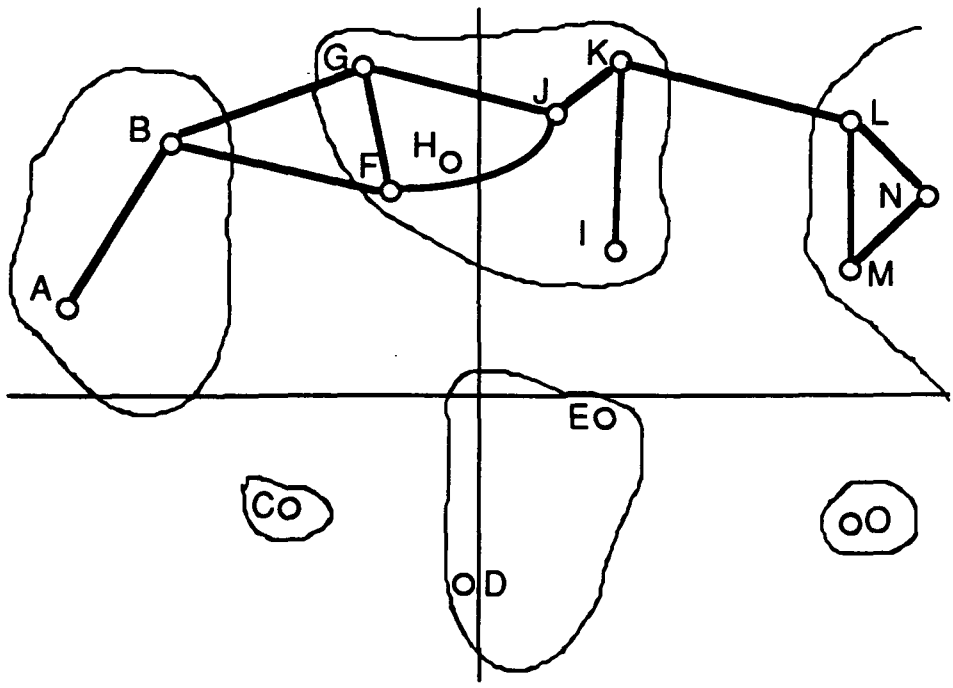

A trade study of the demand for travel along the routes of transportation in Aeroworld was conducted. This study demonstrated that by targeting all continents in the northern half of Aeroworld, we could increase the probability that "*The Initial Guess*" would operate with a full payload for all flights. Figure 1-3 shows the routes which "*The Initial Guess*" will fly.

The next decision in the design process was to determine a range for the "*The Initial Guess.*" The choice of designing a short commuter aircraft was made for several reasons. Since the flight times for a commuter aircraft are shorter than a long range aircraft more flights can be made in a day, thus serving more customers per day. Another advantage of a commuter in Aeroworld is that the greatest demand for travel is between cities near each other. The range of "*The Initial Guess*" was then set at 5500 ft. This range was determined from the longest route that would be traveled with a worst case diversion to an alternate airport and a required loiter time. The cruise flight speed is 28 ft/sec. This velocity provides flight times between 20-45 minutes (AWT) which is much faster than all existing means of transportation. This velocity also corresponds to the minimum power required for the aircraft. A mission endurance of 4 minutes RWT corresponds to a range of 5500 ft. and a cruise flight speed of 28 ft/sec.

The next step taken was to determine a payload. Initially the payload was set at 20 passengers, however it became apparent that in order to offer reasonable ticket prices and still make a profit we would have to increase the payload. We found that with a payload of 56 passengers we could have a very competitive ticket price and make a significant profit.

The final mission requirement is the most important. This requirement is that "*The Initial Guess*" be designed to maximize profit. This can be achieved by keeping the production cost low. The main variable in adjusting the production cost is man hours. Our design will be kept reasonably simple to reduce man hours for production. The most effective way of maximizing profit is to keep operation costs as low as possible. The variables in the operational costs are maintenance and fuel. Fuel cost is the largest expense of operating an aircraft in Aeroworld, and it is therefore necessary for "*The Initial Guess*" to be extremely fuel efficient.

1.7 Key Features

Astro-05: *"The Initial Guess"* power plant is the Astro-05. The Astro-05 is a light weight, efficient propulsion system that is that will provide for maximum fuel efficiency.

Removable Wing: The large rectangular wing removes from the fuselage. This allows for easy access to the batteries, which will reduce maintenance time and cost.

Wing Dihedral: The 9° of wing dihedral provides the roll stability for *"The Initial Guess."* This permits the aircraft to turn by deflecting the rudder.

NACA 4415: The NACA 4415 is an airfoil that has excellent performance at low Reynolds numbers. This airfoil is relatively easy to manufacture and has a very high lift curve slope.

Double-Deck Seating: The seating arrangement of this aircraft allows for comfortable travel, while it maximizes the payload volume. The large number of passengers will generate profit with a reasonable ticket price.

Tail dragger: The tail dragger configuration provides good control characteristics during take-off.

Ticket Price: The ticket price of $75 flat fee and $12/50 ft. is very competitive with the existing means of transportation while it will generate a large profit.

2. AERODYNAMICS AND DRAG

2.1 Aerodynamics

The primary concern of Kappa Aerospace when addressing the aerodynamics and drag of *"The Initial Guess"* was related to finding a configuration that offered a convenient compromise between aerodynamic performance and ease of manufacture. At the same time, the design requirement of simplicity was to be kept in mind throughout the process.

With respect to aerodynamic performance, it was desired that the wing airfoil have both a high maximum lift coefficient and a high lift curve slope (to provide adequate lift at relatively low angles of attack). Airfoil stall characteristics were considered as well; the stall pattern of the airfoil was to show a gradual drop in lift after the maximum lift coefficient is reached. Sudden drops in lift were not desired. Additionally , to avoid problems that occur with low Reynolds Number flight, the geometry of the airfoil was to be chosen correctly. These problems include separation of flow from the airfoil surface. If the airfoil is chosen correctly, a laminar separation bubble is formed over its surface when the previously attached flow encounters a sufficiently strong adverse pressure gradient to cause the flow to separate. There is a process of separation, transition, and reattachment that results in this separation bubble which has a predominant effect on the airfoil flowfield. Thus, it is important to have an airfoil that does not facilitate flow separation if there is a low Reynolds Number flow.

With respect to manufacture, it was desired for the airfoil to have a relatively simple shape in order to reduce construction time and inaccuracies resulting from manufacture. One of the important characteristics for the airfoil was a flat bottom. This feature will enable a more accurate prediction of performance characteristics. Once the airplane is built, it will have a performance closer to its specifications due to the fact that it is easier to manufacture. The main advantage presented by a flat bottom airfoil from the manufacturing point of view comes from the fact that it can be laid down on

a table. This fact is advantageous because a table can then be used as a support to build the airfoils, and further as a means of assuring that all airfoils are aligned in the wing. A round bottom airfoil makes these tasks more involved than a flat bottom airfoil. The flat bottom will increase the chances that a relatively inexperienced construction team can complete the wing successfully.

Most of the airfoils considered for the aircraft were found in 'A Catalog for Low Reynolds Number Airfoil Data for Wind Turbine Applications' (U.S. Dept. of Commerce, National Technical Information Service, Feb 82), available at the Aerospace Laboratory, University of Notre Dame. Airfoils that were found to have a good possibility of meeting the group's requirements were selected for a more intense study. All of these airfoils were of the NACA family. All other airfoils, particularly some with relatively good aerodynamic performance -- high lift coefficient, high lift curve slope -- were discarded because their geometries were too complicated to fulfill our construction requirements. The airfoils selected were the NACA 4412, 4415, and 8318. From these options, the NACA 4415 became the final choice for the aircraft. This decision was based on the better aerodynamic performance of the airfoil, and in the low Reynolds Number reliability advantages of a 15% chord thickness (at the time of choosing the airfoil the flight Re of the aircraft was estimated between 150,000 and 200,000; however this was not a definite range so a conservative position was taken). The aerodynamic characteristics of the chosen airfoil are shown in Table 2-1, and its lift curve is shown in Fig. 2-1. A cross section of the NACA 4415 airfoil is illustrated in Figure 2-2.

TABLE 2-1 Aerodynamic Characteristics of the Airfoil

Airfoil Type	NACA 4415
Chord Thickness	15%
Cl max	1.4
Stall Angle	12°
Lift Curve Slope	0.12 / degrees
Zero Lift Angle of Attack	-4°
Parasite Drag Coefficient	0.0072

Figure 2-1. NACA 4415 AIRFOIL LIFT CURVE

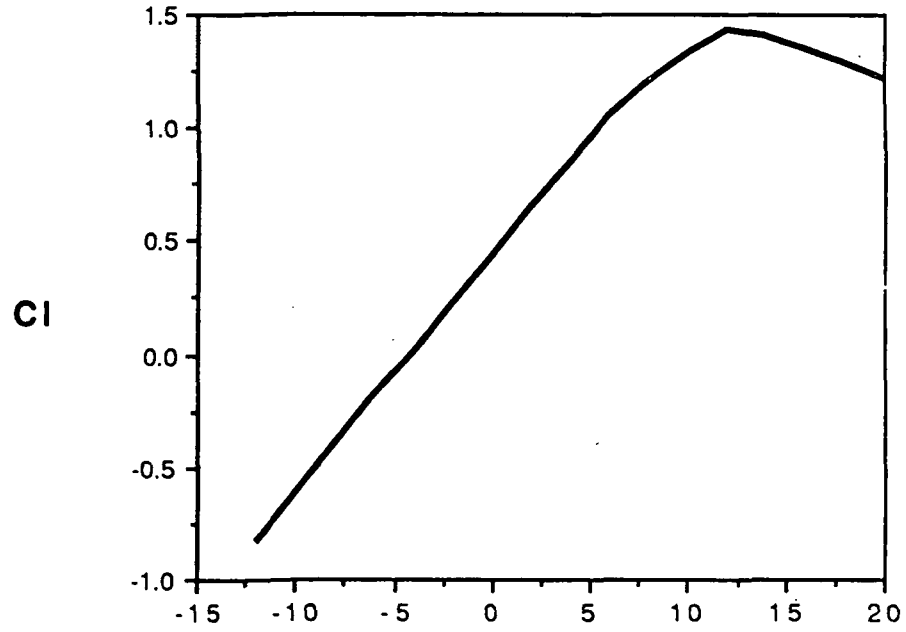

FIGURE 2-2 AIRFOIL SHAPE

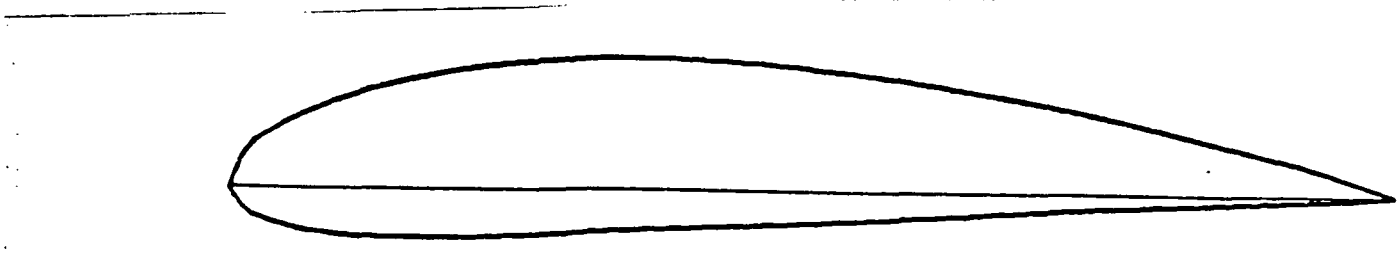

Preliminary calculations for the performance of the aircraft with the chosen airfoil were carried under the assumption that the wing had a rectangular planform area, which simplified the aerodynamic analysis. The span of the aircraft was chosen to be 7 ft in order that the airplane satisfy the design goal of fitting in 7 ft wide airport gates. It would have been possible to hinge the wing with the purpose of increasing span and wing area, keeping the wing chord low and thus reducing induced drag, but this adds weight and complications to the manufacturing process of the aircraft and so the design objective of simplicity would not have been satisfied. The chord of the wing was chosen to be 1 ft for these preliminary calculations, because this is a simple number to calculate with that provided a satisfactory wing aspect ratio of 7. With these wing dimensions, the maximum lift coefficient of the aircraft was found to be 1.05. The initial estimate for the weight of the aircraft was 3.75 lbs, based largely on aircrafts built in past years. A discussion on Weights and Structures is included in Section 4 of this report. With all these aircraft characteristics it was found that the stall speed of 'The Initial Guess' would be 21 ft/s. After it was found that the aircraft would fly with these characteristics, other wing configurations were studied in an attempt to find solutions that provided higher lift with lower drag.

A rectangular wing planform was initially considered because calculations are much simpler than for other wing planforms, and also because it is a planform that offers a convenient stall behavior. The rectangular wing stall exhibits flow separation at the wing root first and then moves outward towards the tip. This is so because of the spanwise lift distribution on the wing. There is a higher percentage of the wing lift concentrated near the root of the wing than near its tip. Other wing planforms considered include elliptic shapes because of their low induced drag, but they were found to be difficult in their construction.

Aspect ratio needs to be kept as high as possible in order for the induced drag to be reduced while the lift of the wing is increased. The span considered for the aircraft is always 7 ft. because it is a design requirement, and therefore the chord is the variable parameter used to vary the aspect ratio. The stall speed and the maximum lift coefficient of the aircraft, together with its weight have a strong effect on the planform area of the wing. Because of the 7 ft wing span

requirement, a variation in wing area strongly effects the aspect ratio of the wing because it must be accomplished through a change in chord length.

After an analysis of the effect of finite wing in lift coefficient was made, a conservative attitude towards the obtained results was taken when inaccuracies introduced by manufacture were estimated. In our preliminary calculations a stall speed of 21 ft/s was thought to be feasible for the aircraft. However, after production was taken into account and previously designed aircrafts were studied, the airplane's maximum lift coefficient was not expected to raise above 0.9 (the theoretical CLmax being 1.05), and the stall speed had to be increased to 23 ft/s. The reason why the altered characteristic of the aircraft was the stall speed and not the wing area was because the latter implied a change in chord length, and this altered significantly the structures and weight analyses performed so far. An increase in stall speed did not influence other aircraft characteristics.

Taper ratio was considered an advantageous characteristic for the aircraft wing because it reduces its induced drag. However, a taper ratio higher than one carries construction disadvantages. The manufacture of a tapered wing would most likely increase construction time and decrease the accuracy of the process, thus not fulfilling the design requirement of simplicity. For our purposes, a wing taper ratio different from one is not desirable.

Another important characteristic of the aircraft is its dihedral angle. This angle, which was calculated to be 9 degrees, was imposed by stability and control requirements since the aircraft does not use ailerons for roll control. The option of using ailerons was discarded because it added difficulties to the manufacturing process of the aircraft. The aircraft uses the rudder to achieve turning flight, which is possible through the dihedral angle of the wing. Thus, it is necessary to have a dihedral angle in the wing to have roll control, as well as to improve the static stability of the aircraft. A discussion on stability and control for the aircraft is included in section 5 of this report.

Finally, it was necessary to calculate the angle of incidence of the wing on the fuselage so that the aircraft could have a cruise flight at an efficient angle of attack. To find the mount angle of the wing, it was necessary to find a

compromise between the ratio of lift over drag and lift coefficient values. The reason why such compromise had to be sought is because the highest lift over drag ratios occured when lift coefficient values were below those desired for cruise flight. The reason why low lift coefficient values were a concern for the aircraft's cruise flight is because its cruise speed became higher than desired due to engine performance limitations. A discussion on the propulsion of the aircraft follows in the next section of this report. The aircraft's lift curve is presented in Figure 2-4, and the lift to drag ratio curve for increasing angles of attack is given by Figure 2-5. The angle of incidence was chosen to be 3 degrees, which allows the aircraft to fly at a cruise speed of 28 ft/s.

The final wing configuration is summarized in Table 2-2.

TABLE 2-2 AIRCRAFT WING CONFIGURATION

Wing Area	1008 in^2
Wing Span	84 in
Wing Chord	12 in
Aspect Ratio	7
Maximum Lift Coefficient	1.05
Expected Real Maximum Lift Coeff	0.9
Stall Angle of Attack	8°
Stall Speed	23 ft/s
Taper Ratio	1
Dihedral Angle	9°
Cruise Speed	28 ft/s
Cruise Angle of Attack	3°

FIGURE 2-4. AIRCRAFT LIFT CURVE

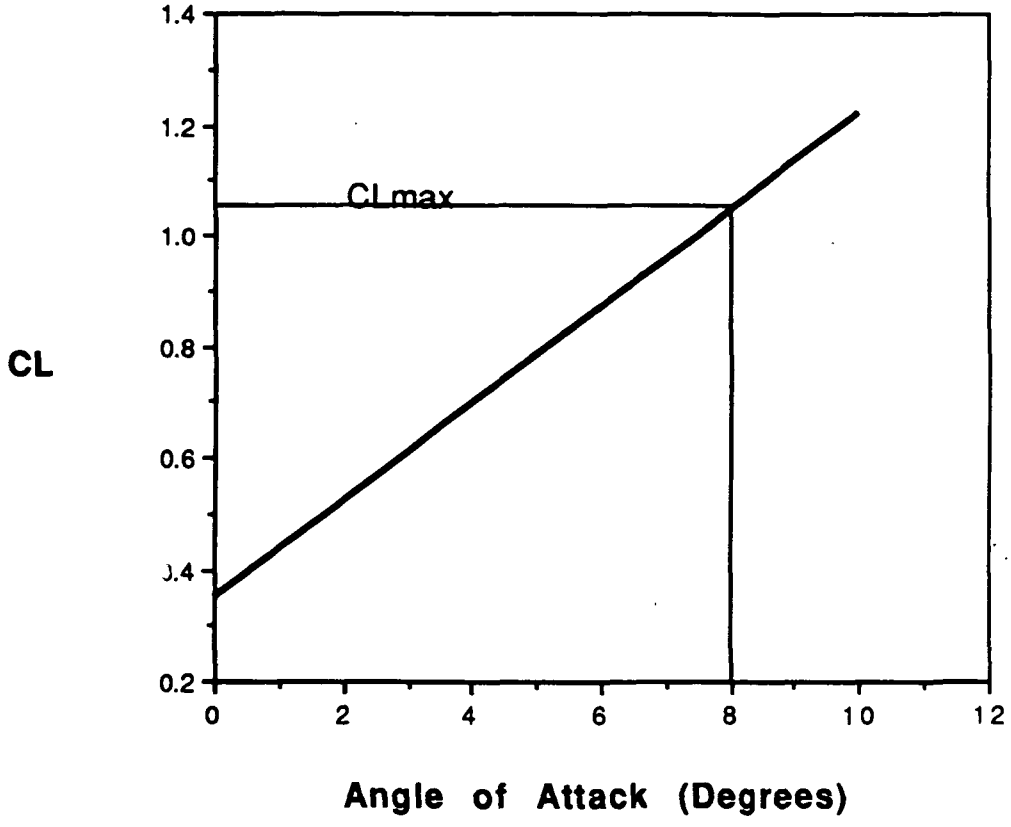

FIGURE 2-5. LIFT TO DRAG RATIO vs. ANGLE OF ATTACK

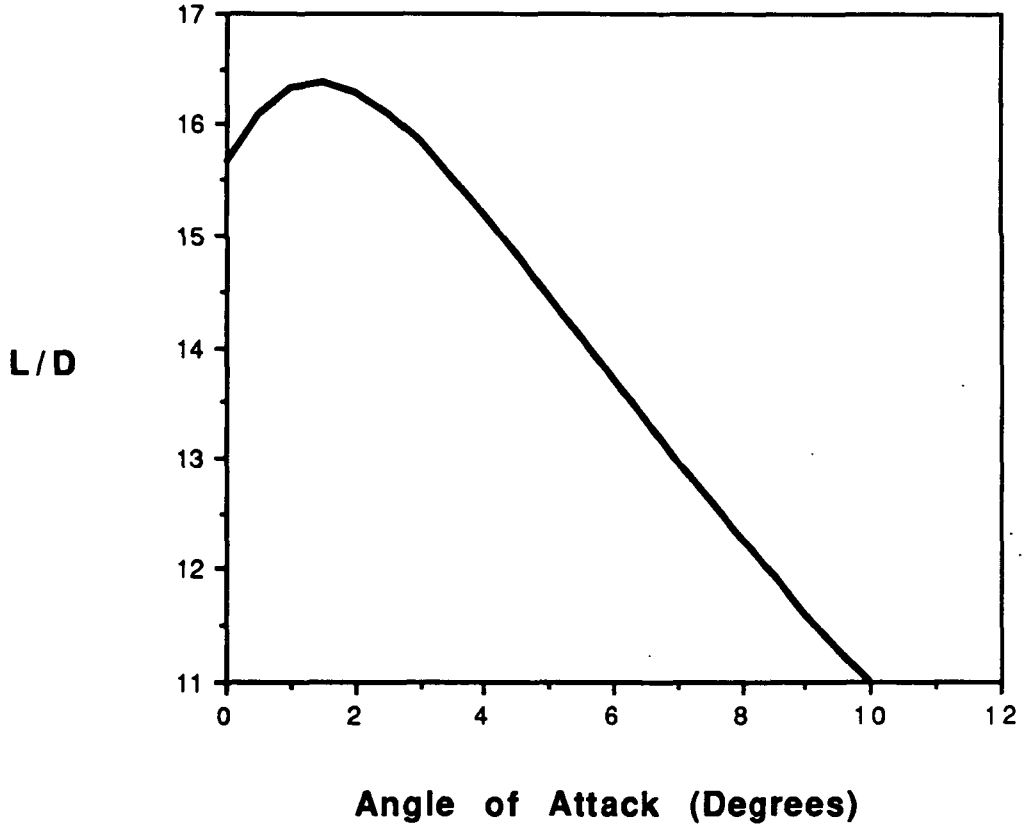

2.2 Drag

The drag prediction for our aircraft was completed using the drag breakdown method as presented by Dr. Robert Nelson in his pamphlet detailing this subject. According to the procedures outlined in Dr. Nelson's pamphlet, our aircraft was broken down into five components: wing, fuselage, horizontal tail, vertical tail, and landing gear. For each component, a characteristic area, A_π, was calculated. This area was then multiplied by the component drag coefficient, $C_{d\pi}$, that was supplied in the pamphlet. When this had been completed for each of the five parts, the drag components were summed. This summation was then used in the equation for C_{do}: $C_{do} = (1/S_{ref})*\Sigma(C_{d\pi}*A_\pi)$. For our aircraft the S_{ref} value was the wing area, 7.0 square feet. The component breakdown, the values of $C_{d\pi}$ and A_π, and the percentage contribution of each component are presented in Table 2-3. It should be noted that the two components which yield the largest percentage of the drag are the wing and landing gear. For our aircraft, the value of Cdo was calculated to be 0.029.

Table 2-3. Drag Component Breakdown

Component	C_{dp}	Ap	C_{dp}*Ap	Percent
Wing	0.007	7.000	0.049	23.8
Fuselage	0.110	0.174	0.019	9.2
Horiz Tail	0.008	1.778	0.014	6.8
Vert Tail	0.008	0.625	0.005	2.4
Landing Gear	0.017	7.000	0.119	57.8
			0.206	100.0

In addition to finding C_{do}, it was also necessary to calculate the plane's efficiency factor, e, in order to calculate the complete drag polar for the aircraft. This was accomplished by using the equation $e = 1.78*(1-0.045*(AR)^{0.68}) - 0.64$, as supplied by the Master's thesis of Mr. Dan Jenson, University of Notre Dame. For our aircraft this produced a value of 0.83 given our aspect ratio of 7. In order to account for interference and roughness effects, this value was reduced by 15%, as suggested by Dr. Nelson in his drag prediction pamphlet; this gave us our final value of e = 0.71.

Using the values predicted by the drag breakdown method and the above equation, the complete drag polar function for the aircraft was found to be $C_d = 0.029 + 0.0648\ C_l^2$. This function, which is represented in Figure 2-6, is expected to represent an accurate estimate of the drag exerted on by the air on the aircraft.

FIGURE 2-6. AIRCRAFT DRAG POLAR

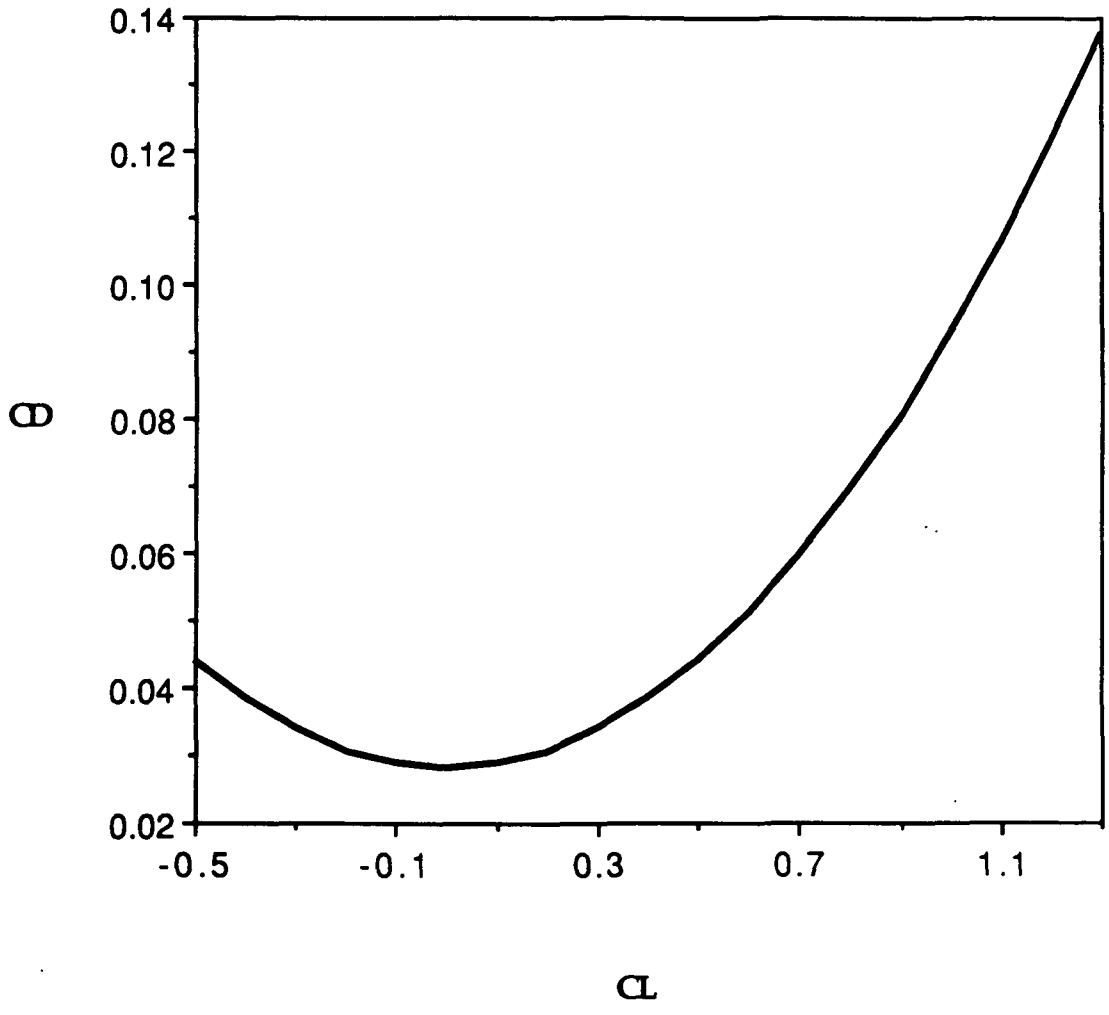

3. PROPULSION

3.1 Motor Selection

One of the primary components of any aircraft is its mode of propulsion. The propulsion system had to be chosen from a family of specified motors. This family of motors was the Astro line, which consisted of the following models: Cobalts 035 - Cobalt 40, and the FAI 05. Other means of propulsion were eliminated from our aircraft by the rules of Aeroworld.

To select which member of this family our aircraft would use, we had to look at the design requirements we had previously formulated for the mission of our aircraft. The goal of primary importance to Kappa Aerospace was to design a transport capable of yielding the greatest potential return on our investment in the new airline market of Aeroworld. To accomplish this task, we sought to minimize as many of our operating costs as possible. The most significant operating cost of our aircraft is the cost of fuel. The aircraft fuel approved for use in Aeroworld ranges between $60 and $120 per milli-amp hour used. Thus, for example, draining a 1200 milli-amp hour fuel cell will cost the airline between $72,000 and $144,000. These totals far exceed any other daily operating cost and will quickly surpass the production cost of each aircraft. Therefore, the ideal propulsion packet for our aircraft would be one capable of supplying enough power to take-off and maintain flight while drawing a minimum amount of current. In addition to the low current draw requirement, we also sought to keep the total weight of our aircraft below 60 oz., meaning that the lighter the motor the better. From rough, initial calculations, only three motors were selected to be looked at more closely. These three motors were the Astro 035, Astro 05, Astro 15; the others were eliminated primarily for high current draws, too much power available, and excessive weight.

For the remaining three motors, a performance spread sheet was developed which calculated power available, power required, and amp-hour usage. Initial data from the Astro Motor Performance tabulations were used to

perform the necessary calculations. To obtain the above quantities, a propeller was selected to serve as a base means of comparing the motors. A sample of this spread sheet is provided to quantitatively show this data in Appendix A for the Astro 05 motor and the Zinger 10-6 propeller. From the performance spread sheet, data was obtained to evaluate and compare the Astro 035, Astro 05, and Astro 15. The analysis revealed that the Astro 035 burned too much fuel to sustain steady level flight to meet our design goal of low current-draw. In addition to this draw back, the 035 would not be capable of providing the necessary excess power available should our aircraft encounter the need to climb. Consequently, the Astro 035 was eliminated from consideration despite its desirably low weight. The Astro 15 was also eliminated after the analysis, even though it exhibited the lowest current draw of the three motors. It was found that the Astro 15 was too powerful for our aircraft configuration, to the point where this excess power was inefficient based on the weight penalty incurred by using the 15. Thus, a trade-off between the beneficial characteristics of the 035 and the 15 were obtained through the Astro 05.

The Astro 05 meets all of our relevant design requirements without a weight penalty or an inefficient production of power. The 05 allows us to maintain steady level flight while only drawing 3.33 amps. Because the Astro 05 does not supply our aircraft with a surplus of power as the Astro 15 does, the production of our aircraft will have to be extremely rigorous so as not to exceed the weight and drag estimations made during the design phase of the production of our aircraft.

The desired range and take-off performance of our aircraft governed to a large extent the type of batteries that our aircraft would implement. The battery pack had to be capable of delivering the maximum amount of power to the motor to enable our aircraft to take-off within the specified 60 ft runway length. (See appendix E2 for take-off calculations) The battery pack also had to have enough capacity to supply the motor with the 3.33 amps needed throughout the cruise flight. It was decided that the fuel for the Astro 05 would consist of 10 panasonic 1.1 amphr capacity batteries. Thus giving *"The Initial Guess"* sufficient battery capacity and voltage drop.

3.2 Propeller Selection

The selection of a propeller is just as crucial as the selection of a motor for our aircraft. The two primary considerations in selecting a propeller for our aircraft are the availability of the prop and the efficiency of the prop. To ensure that there would be ample supply of our selected propeller, we limited the props which we examined to those readily available over-the-counter at most hobby shops. Props looked at included: TopFlight 9-4; Airscrew 12-6; Zinger 8-6, 10-6, 12-6,13-7, 14-8. Plots of efficiency versus advance ratio for these props were obtained from references [3] and [5]. The data points of these graphs were recorded in a Cricket Graph file and plotted. The plot could then be curve fit to obtain an equation for the propeller efficiency. These are the functions which were then entered into the spread sheet for the Astro 05 motor to obtain the performance values of the motor/prop combinations.

To ensure that a maximum amount of the power out from the motor is converted to power available, it is best to select a prop which exhibits relatively high efficiency over the range of operable advance ratios. For our aircraft, it was found that the prevalent range of advance ratios was between 0.1 and 0.3, roughly. For this range of advance ratios, the two best propellers turned out to be the Zinger 10-6 and the Zinger 12-6. Currently, our aircraft uses the Zinger 10-6 because of its high efficiency (See Fig.3-1).

The Zinger 12-6 is still under serious considerations for use in our aircraft for many reasons. Despite its lower efficiency, the 12-6 may still be implemented because the 12 in. diameter is capable of providing more thrust should our drag be underestimated. Another aspect of propeller performance which is directly effected by the prop diameter is the loss of performance due to blockage. Our fuselage is 5 in. by 5 in. and thus can provide considerable blockage for a 10 in. diameter prop. Construction plans call for a tapered fuselage in the front, but the maximum possible taper down is to the minimum diameter needed to be able to easily remove the motor from its casing. Therefore, blockage effects will have a significant effect upon the propulsion packet's performance. As we have come across no method of estimating the effect of blockage, the performance spread sheet reduces the power available by 40% to compensate for blockage effects. The validity of the

Figure 3-1

Propeller: Zinger 10-6

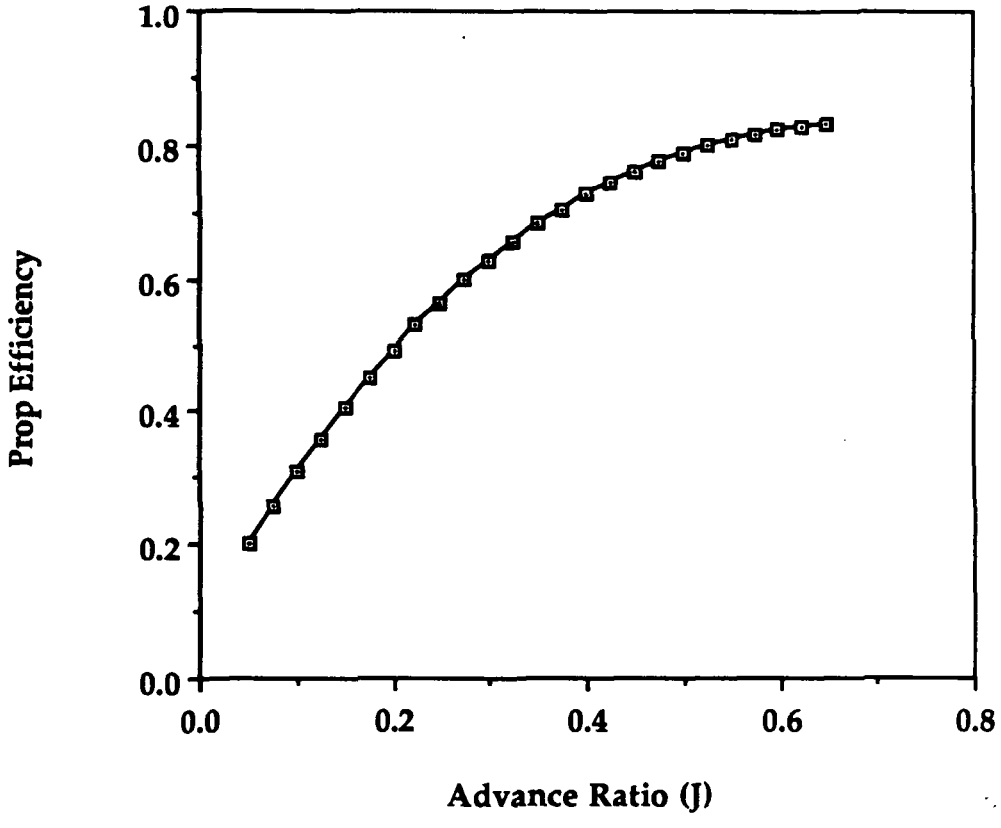

estimated effect of blockage will be determined in the taxi tests. If blockage sufficiently reduces the available thrust, then the Zinger 12-6 will be implemented. To ensure that this possible propeller change does not require considerable design adjustments, the landing gear will be designed to provide enough ground clearance for the 12 in. prop. Changing the prop will have negligible effect on the center of gravity due to the similarity of the weight of the two props. Consequently, our aircraft's propulsion packet consists of an Astro 05 motor with 0.8 amp-hours of battery capacity and the Zinger 10-6 propeller.

3.3 Motor/Prop Performance

The combination of the Astro 05 motor and the Zinger 10-6 propeller yields very good performance characteristics for our aircraft. The light weight motor is more than capable of providing enough power to take-off and maintain flight. The power available versus power required curves for our aircraft can be seen in Figure 3-2. As can be seen by the maximum power available curve, our aircraft can withstand a three-fold increase in the power required and still

Figure 3-2

Power Available vs. Power Required
Motor: Astro 05
Propeller: Zinger 10-6

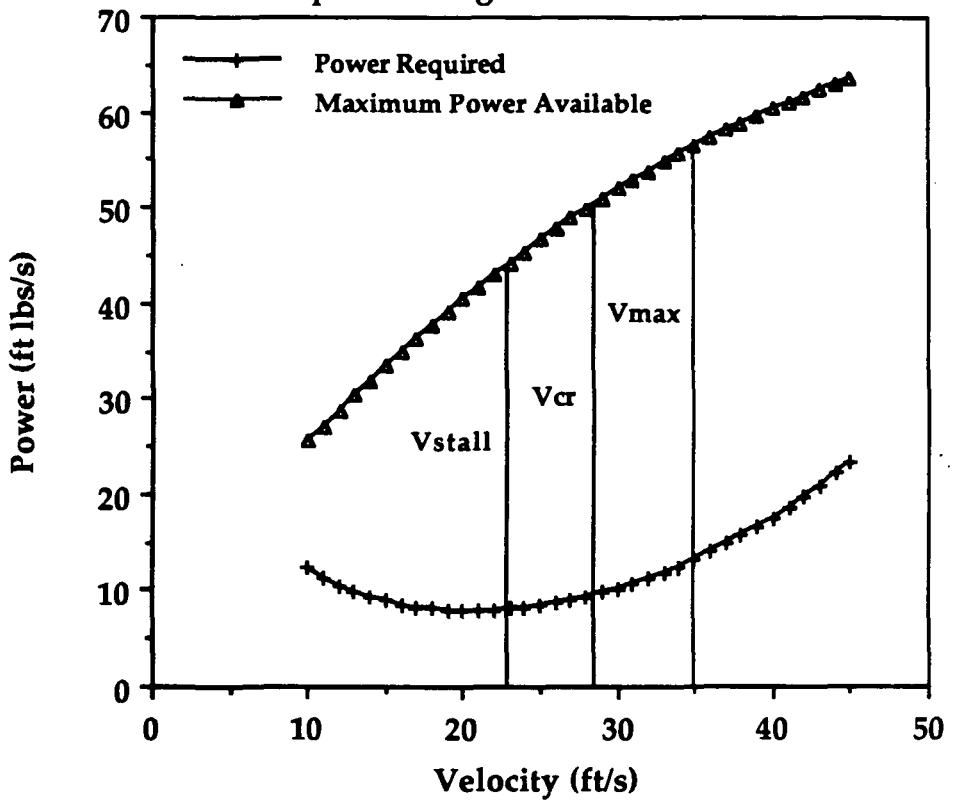

be able to maintain steady level flight. The range of operable velocities for our aircraft is set by a minimum at V_{stall}, 23 ft/s, and a maximum speed in Aeroworld of 35 ft/s. Consequently, at the above power setting, the maximum range of velocities is traversable with positive rate of climb capabilities. Figure 3-3 shows the battery drain when flying at various forward velocities. Our aircraft will cruise at 28 ft/s and at 0 ft/s rate of climb. These two conditions yield an amp-hour drainage of 0.11 amp-hours to fly

our design range of 5500 ft. Additional calculations were made to estimate the performance of our aircraft, and can be found in Section E - Performance.

In conclusion, adequate power supplies are achieved using the Astro 05 motor without realizing a weight penalty. Low current draw for the motor for our range of operating conditions enables us to minimize the daily fuel costs for operation of the airline. Care will have to be taken in construction of the aircraft so as to keep the drag and weight of the aircraft within reasonable agreement of the estimated values.

Figure 3-3

Battery Drain for Cruise and Rate of Climb Conditions at Various Forward Velocities

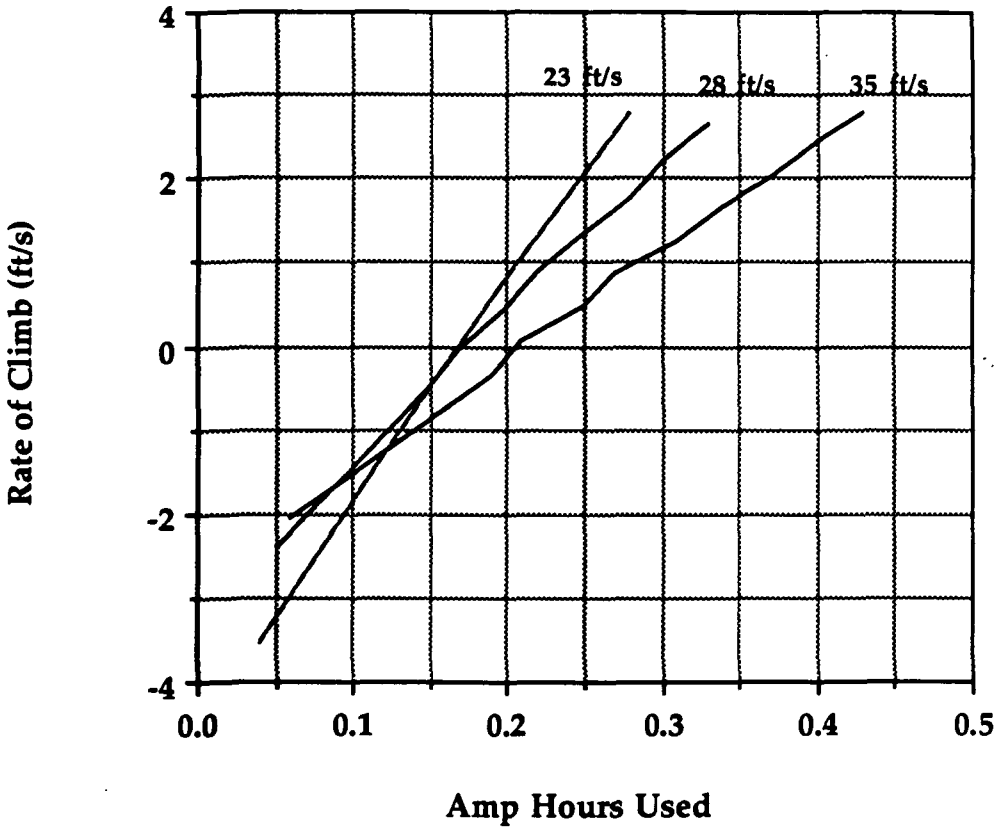

4. WEIGHTS ESTIMATION AND CENTER OF GRAVITY LOCATION

4.1 Weight Estimation

When the design process began, preliminary specifications of *"The Initial Guess"* were developed. The large database of RPV's designed at the University of Notre Dame was used to select component weights which would closely reflect the final weight values. These initial values heavily influenced the selection of the power plant for the aircraft. The initial weight estimation is very difficult to achieve with great accuracy because it is only an "initial guess" as to what the aircraft will weigh after production. The initial weight estimation of the aircraft was 60 oz. The estimation of the weight changed throughout the design process as many of the details varied. After all the details of the aircraft were finalized, the weight estimation of the aircraft was also 60 oz. The initial and final estimations of the aircraft weight were the same, however the final component weights were different from the initial component weights. The breakdown of the component weights and the percentage of their weight to the weight of the entire aircraft is shown in Table 4-1.

The final estimation of the weight of the aircraft will also vary from the weight of the aircraft after production. This is due to the fact that the estimations of the weight of the aircraft were based on the average density of the type of wood being used and also because the weight of the glue and the monokote was excluded. Another difficulty is that any unforeseen design modifications which must be corrected during the production are not included in the weight prediction.

Table 4-1

COMPONENT	WEIGHT (oz.)	WEIGHT %
PROPELLER	1.00	1.6%
ENGINE	6.50	10.7%
ENGINE MOUNT	1.14	1.9%
BATTERIES (ENG.)	6.24	10.3%
BATTERIES (SYS.)	2.00	3.3%
RECEIVER	0.95	1.6%
SERVOS	1.20	2.0%
SPEED CONTROLLER	3.23	5.5%
WING	10.00	16.5%
FUSELAGE	11.80	19.5%
EMPENNAGE	5.00	8.3%
LANDING GEAR	7.00	11.6%
PAYLOAD	4.94	8.2%

4.2 Center of Gravity Location

Knowledge of the location of the center of gravity is a crucial part of the stability of the aircraft. If the center of gravity is too far aft, then the aircraft will become unstable, and if the location is too far forward then the aircraft will not have enough control power to take-off or land. The location is determined by using the knowledge of the center of gravity locations and the estimation of the weights for all components. The following equation was used to determine the center of gravity location.

$$X_{c.g} = \frac{\sum_{i=1}^{i=13} X_{c.g.i} * W_i}{\sum_{i=1}^{i=13} W_i}$$

A spreadsheet program (included in appendix B) was written to determine the center of gravity locations along both the length and width of the aircraft. The following table gives the weights of each component and their center of gravity locations.

Table 4-2

* All distances are referenced from the propeller.

COMPONENT	WEIGHT(oz.)	C.G. LOCATION (in.)
PROPELLER	1.00	0.0
ENGINE	6.50	3.13
ENGINE MOUNT	1.14	4.25
BATTERIES (ENG.)	6.24	8.75
BATTERIES (SYS.)	2.00	6.62
RECEIVER	0.95	7.59
SERVOS	1.20	6.41
SPEED CONTROLLER	3.23	4.94
WING	10.00	17.0
FUSELAGE	11.80	20.7
EMPENNAGE	5.00	48.0
LANDING GEAR	7.00	12.7
PAYLOAD	4.95	39.0
TOTAL		
NO PASSENGERS	55.50	12.61
FULL PAYLOAD	61.01	13.78

The initial location of the center of gravity location was at almost 40% of the chord, which would give *"The Initial Guess"* poor handling qualities. The neutral point location of the aircraft is 16.4" from the nose of the aircraft. It was necessary to either move the center of gravity forward or change the

location of the neutral point. Changing the neutral point would have required varying the tail size or the distance of the tail from the wing. After researching methods of changing the handling qualities of the aircraft, it was determined that the most effective way to accomplish this was to move the center of gravity. However, even this was not an easy task since we had already positioned all components in a configuration which produced the most forward c.g. location. The wing could have been moved aft to reduce the distance between the center of gravity and the neutral point. This would have been counter-productive since that would also move the center of gravity location further aft. Moving the wing aft would also cause a destabilizing effect since the tail moment arm would be reduced. Another possibility was to add ballast to the front of the aircraft. However we were concerned with keeping the total weight as low as possible since the propulsion system chosen was not extremely powerful. The most effective way of moving the center of gravity was to add one inch of fuselage length in front of the wing. This addition moved the aircraft center of gravity forward approximately one and a half inches. The new center of gravity location yielded the following values: $X_{n.p.}/c$ = 21.8% (forward), 31.7% (aft); and static margins of 22.9% (forward), 12.2% (aft). The new center of gravity location static margins represent good handling qualities whether the aircraft was either full or empty of passengers.

The travel of the center of gravity was another very important consideration. The center of gravity travel is only a function of payload. The fuel weight does not vary since it is a battery pack which does not change weight. The center of gravity travels 1.2 inches when the passenger load varies from 0 to 56. Figure 4-3 shows the weight and center of gravity locations of the components as well as for the entire aircraft.

Figure 4-3

* The forward center of gravity location represents the case of no payload while the aft center of gravity location represents maximum payload.

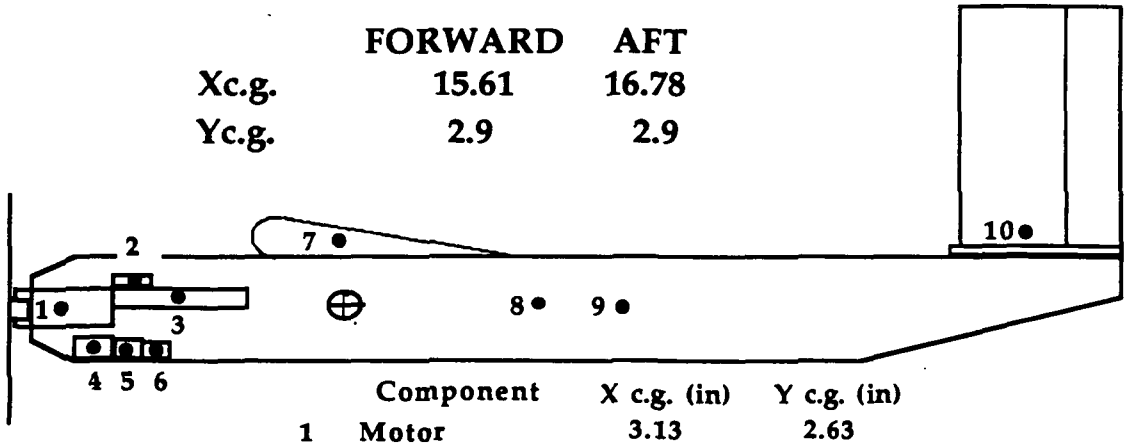

	Component	X c.g. (in)	Y c.g. (in)
1	Motor	3.13	2.63
2	Sys. Battery	6.62	3.50
3	Eng. Batteries	8.75	3.38
4	Spd Controller	4.94	0.63
5	Servos	6.41	0.56
6	Receiver	7.59	0.41
7	Wing	17.0	5.60
8	Fuselage	20.7	2.80
9	Payload	28.0	2.50
10	Empennage	48.0	6.20

4.3 Passenger Seating Configuration

The passenger seating arrangement includes two decks and two rows. This arrangement allows for the maximum use of the payload volume, while still allowing plenty of room for passenger comfort. The need for carrying as many passengers as the volume of the aircraft is extremely important in order to keep the ticket prices low. The ticket price was set at $75 flat fee and $12 per 50 ft. This ticket price is very competitive with the existing means of transportation and also generates substantial profit for the airline. The internal seating arrangement is diagramed in the Figure 4-4.

Figure 4-4

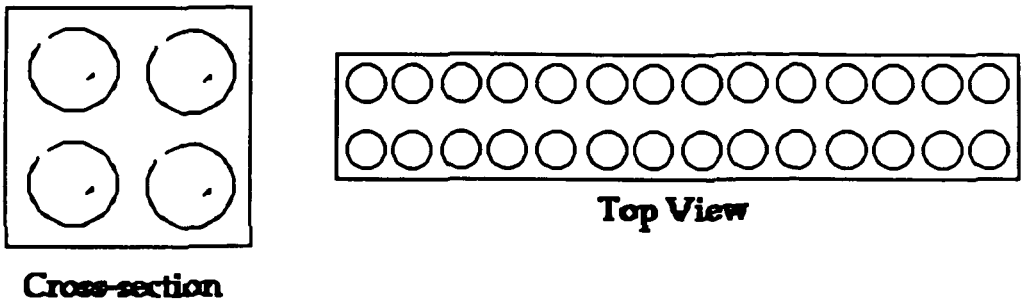

5. STABILITY AND CONTROL

The types of stability that we are concerned with for this aircraft are longitudinal static pitching stability and lateral stability. The main design variable that influences this is the stick fixed static margin. However, this is in turn most affected by the size and location of the aircraft's vertical tail and the c.g. location. We initially estimated that we needed a static margin of 10 to 15 percent of the wing chord. The other driving factor for design of a longitudinal control system was to trim at the desired angle of attack. Section 5.1 will present the governing equations of this analysis while its subsections present our design results and the reasoning behind them. Section 5.2 will present the governing equations of directional stability and control. Finally, section 5.3 will present the roll stability and control using wing dihedral without the use of ailerons. All numerical results for stability and control were calculated directly from the governing equations using a standard spreadsheet format.

5.1 Longitudinal Stability and Control

The primary desire of achieving sufficient longitudinal stability can be insured by having a static margin of at least 10%, depending on the type of aircraft. This static margin can be accomplished by proper sizing of the horizontal tail surface. The horizontal tail also allows the aircraft to be trimmed at a small angle of attack. The aircraft must have adequate longitudinal stability to allow a ground based pilot to easily control the airplane. On the other hand the static stability can not be so great as to impair the maneuverability of the aircraft.

The longitudinal pitching moment coefficient, Cm, can be broken down into several components. These components consist of the contributions of the fuselage, wing, and horizontal tail. Also, because the vertical moment arm from the center of gravity to the wings drag vector is not negligible for our aircraft, the contribution to the drag is also included. A flat plate is used for the horizontal tail because other thin airfoil geometries have little effect on the efficiency of the tail. From thin airfoil theory, the lift slope is 2π which is

then corrected using the tail aspect ratio. The following, taken from Reference [8], are the governing equations for Cm :

$$Cm_{cg} = Cm_o + Cm_\alpha \alpha$$

$$Cm_\alpha = Cm_{\alpha_f} + Cm_{\alpha_w} + Cm_{\alpha_t} + Cm_{\alpha_D}$$

$$Cm_o = Cm_{o_f} + Cm_{o_w} + Cm_{o_t} + Cm_{o_D}$$

The component contributions can be found in Appendix C.

5.1.1 Stick Fixed Neutral Point and Static Margin

The stick fixed neutral point is defined as the center of gravity position where the aircraft is neutrally stable. Thus the neutral point is found by setting Cm_α equal to zero in the pitching moment equation. If the center of gravity is moved aft of this point the aircraft will be statically unstable. The stick fixed static margin is the distance between the actual center of gravity and the neutral point. The following are the equations for the neutral point and static margin, respectively :

$$\frac{X_{NP}}{\bar{c}} = \frac{X_{ac}}{\bar{c}} - \frac{1}{C_{L_{\alpha w}}} (Cm_{\alpha f} + Cm_{\alpha t} + Cm_{\alpha D})$$

$$S.F.S.M. = \frac{(X_{NP} - X_{cg})}{\bar{c}}$$

5.1.2 Horizontal Tail Design

The primary design variables for longitudinal stability and a small trim angle are the volume ratio, horizontal tail planform area and aspect ratio, horizontal tail incidence angle, and the tail moment arm. Due to the structural design of the aircraft, the tail moment arm was assumed to be approximately constant for a particular c.g. location. Our aircraft is a passenger transport, which at some time will operate both at and between the most forward and most aft c.g. locations. The forwardmost c.g. location represents the case where there are no passengers aboard. While the most aft

location represents the fully loaded case. The forwardmost c.g. location is at 21.8% of the wing chord, and the aftmost location is at 31.7% of the chord. With the moment arm effectively fixed, the volume ratio becomes a linear function of the horizontal tail planform area. This can be seen in Figure 5-1 with the final design results designated with arrows. The tail chord had to be at least 7 inches to avoid the increased drag of a low Reynolds number. Therefore the tail chord was initially sized at 8 inches, but upon examining the sensitivity of the tail chord on static margin, a chord of 7.5 inches was decided upon. The tail incidence angle was found to have no effect on the longitudinal stability, but instead only on the trim conditions. This left the tail area as the main variable to examine. The aft c.g. location is the limiting case so this was the only location used in most of the following analyses of Chapter 5.

Figure 5-1 Horizontal Tail Volume Ratio vs Horizontal Tail Area

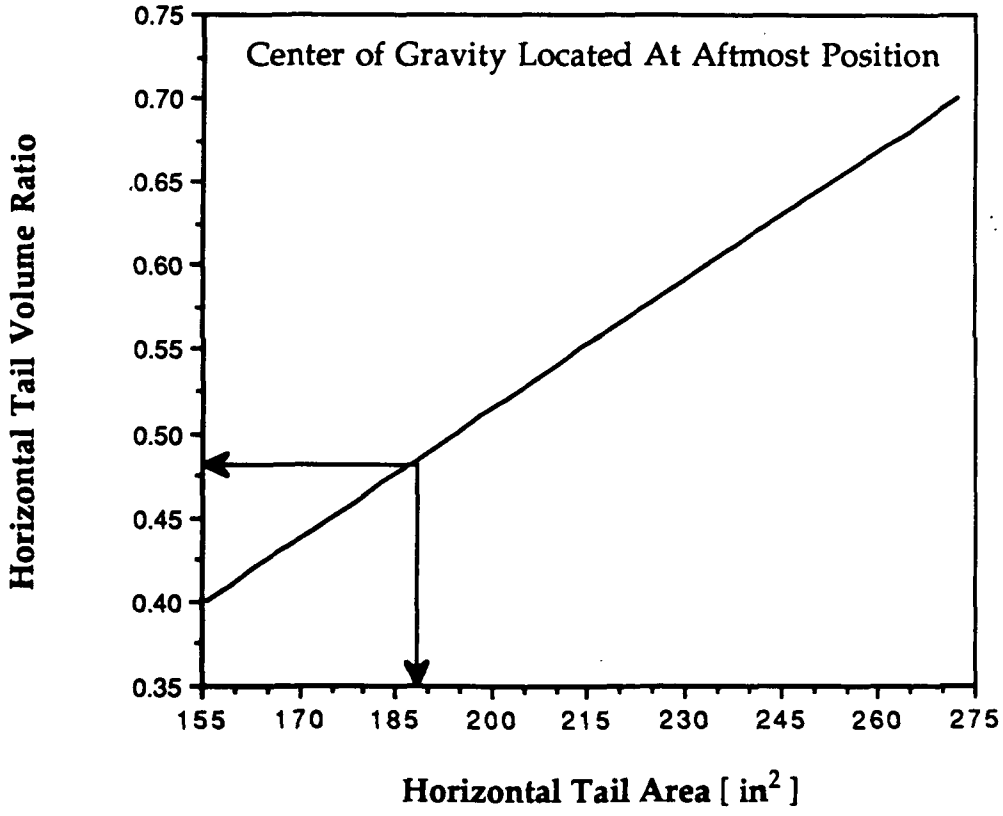

Since the tail incidence angle does not effect the longitudinal stability, the neutral point and static margin are also unaffected. These are therefore linear functions of the horizontal tail area. Figure 5-2 shows the variation in Cm_α for a range of tail areas.

Figure 5-2 Cm_α vs Horizontal Tail Area

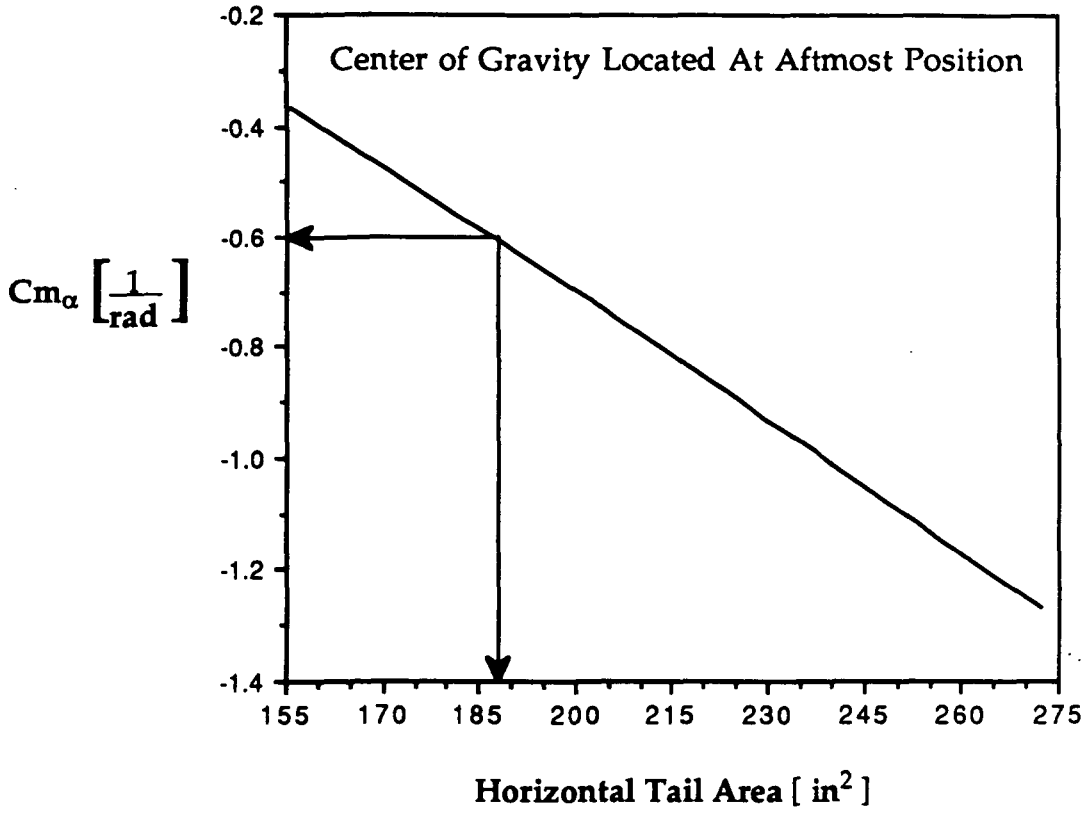

Figures 5-3 and 5-4 show how the neutral point and static margin are influenced by the tail area. The final design results are noted in the figures.

To trim the aircraft at a low angle of attack, the value of Cm_o had to be small. Cm_o is a function of both the tail area and the incidence angle. Figure 5-5 presents the variation in Cm_o with tail area and incidence angle. Figure 5-6 displays the total lift, that due to both the wing and the tail, with tail area and incidence angle. The final design decided upon has a tail area of 187.8 in^2. Thus a tail incidence angle of at least -1.0° is required to provide the 3.74 lbs of lift needed. The tail incidence angle was in fact chosen to be -1.0°, in order to

Figure 5-3 $\frac{X_{NP}}{\bar{c}}$ vs Horizontal Tail Area

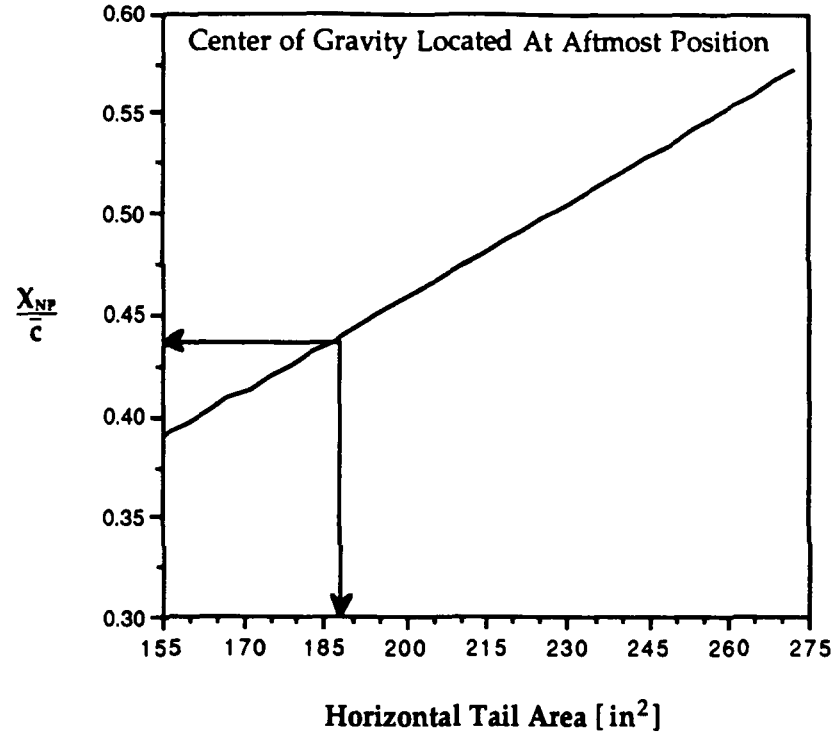

Figure 5-4 Static Margin vs Horizontal Tail Area

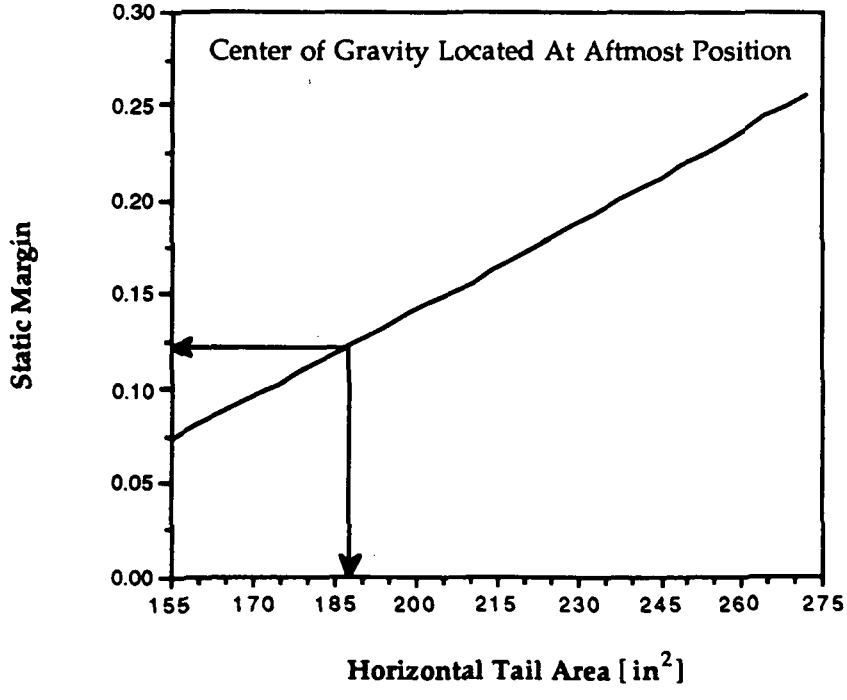

Figure 5-5 Cm_o vs Horizontal Tail Area

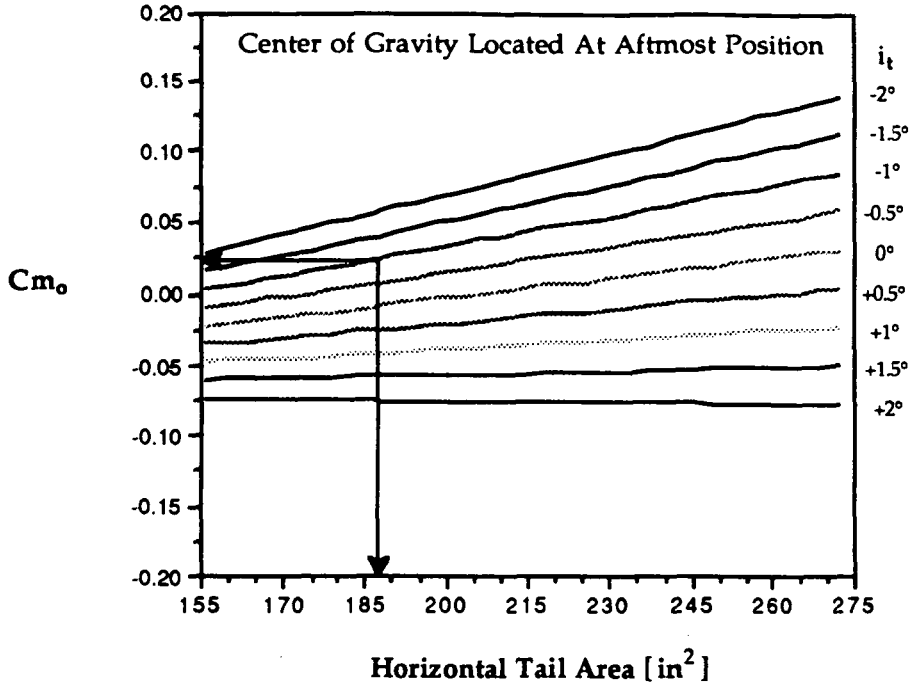

Figure 5-6 Total Lift vs Horizontal Tail Area

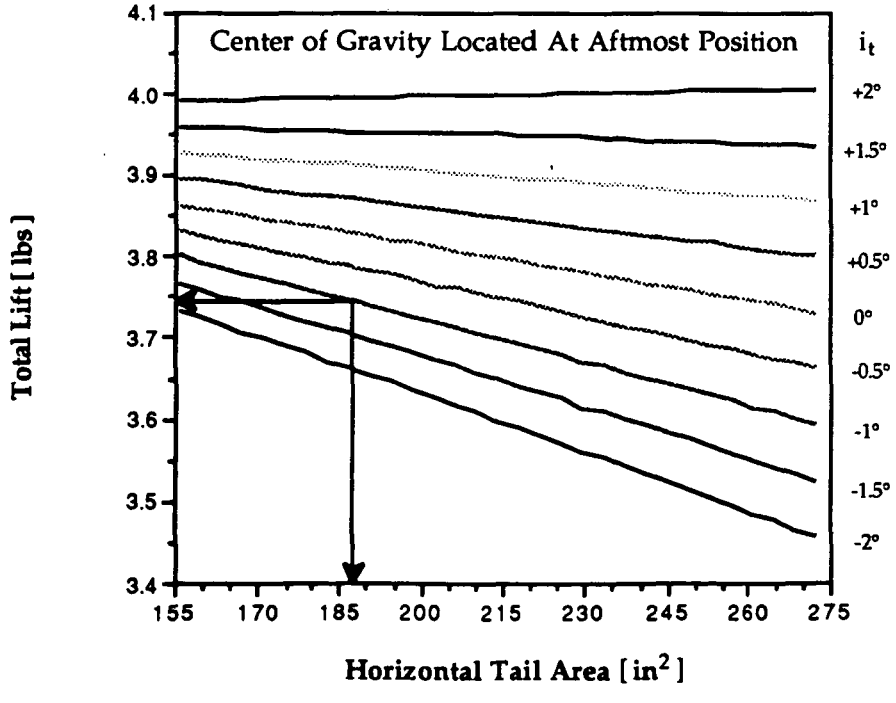

trim, with stick fixed, at a zero degree angle of attack for the forwardmost c.g. location. This also gave a total lift at cruise that was exactly equal to the weight of the aircraft. Table 5-1 contains the final design characteristics of the horizontal tail surface and the longitudinal stability for the forwardmost and aftmost c.g. locations.

Table 5-1 Horizontal Tail Characteristics and Longitudinal Stability

C.G. Location	Fowardmost	Aftmost
X_{cg}/c	21.8%	31.7%
Moment Arm	32.3 in	31.1 in
Volume Ratio	0.501	0.483
Planform Area	187.8 in^2	187.8 in^2
Chord	7.5 in	7.5 in
Span	25 in	25 in
Incidence Angle	-1.0°	-1.0°
Aspect Ratio	3.34	3.34
Cm_α	-1.141 rad^{-1}	-0.607 rad^{-1}
Cm_o	-0.007	0.024
X_{NP}/c	44.6%	43.8%
Static Margin	22.9%	12.2%

Figure 5-7 shows the pitching moment coefficient as a function of angle of attack for the final design conditions at both the forwardmost and aftmost c.g. locations. The static margin at the aft c.g. location is 12.2%. This should provide good longitudinal stability without impairing maneuverability.

5.1.3 Elevator Sizing

The elevator was sized using the following equations from Reference [8] :

$$Cm_{\delta_e} = \frac{\Delta Cm_{max}}{\delta_{e_{max}}}$$

where ΔCm_{max} is found from the greater of the ΔCm required to trim the aircraft at landing or the ΔCm to rotate the aircraft during take-off.

Figure 5-7 Cm vs Angle of Attack

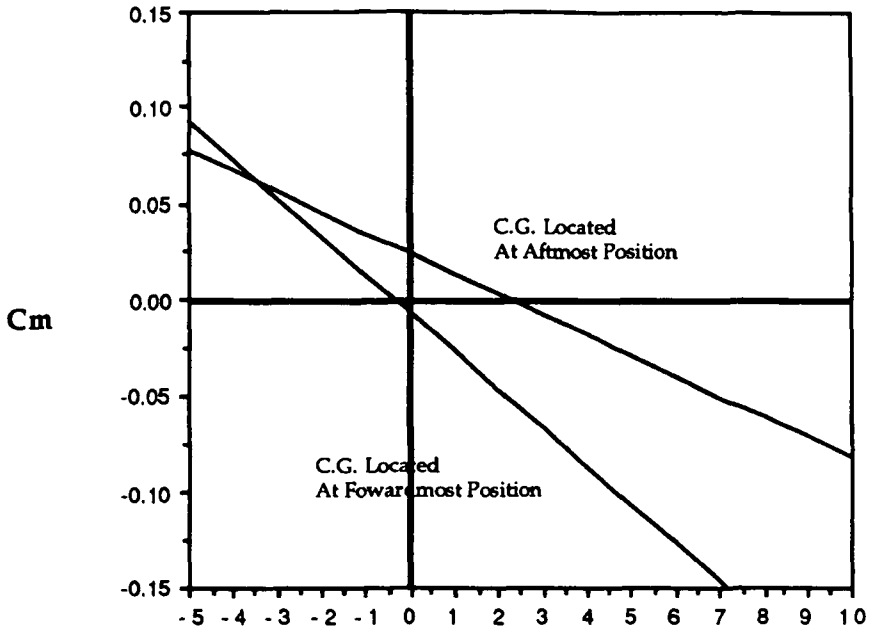

Figure 5-8 Cm vs Angle of Attack

Center of Gravity Located At Aftmost Position

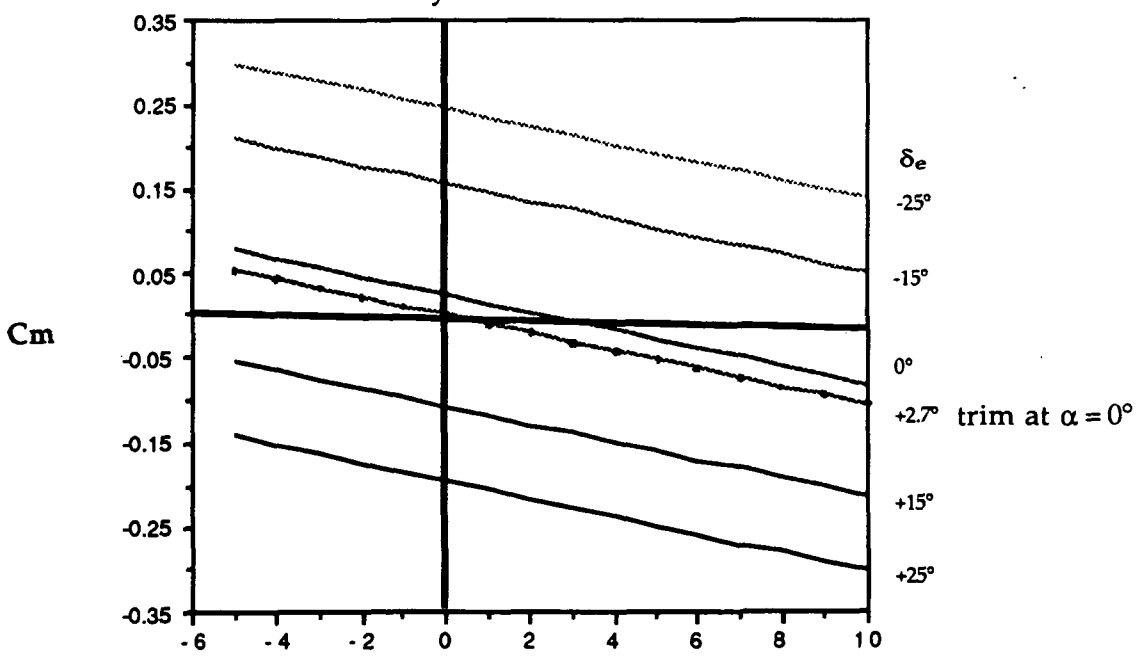

$$Cm_{\delta_e} = -\eta V_H C_{L_\alpha} \tau$$

Using the equation below the elevator effect on the pitching moment was determined. Figure 5-8 , for the aft c.g. location only, shows that the aircraft can be trimmed at zero angle of attack with a elevator deflection of +2.7°.

$$Cm = Cm_o + Cm_\alpha \alpha + Cm_{\delta_e} \delta_e$$

Table 5-2 shows the elevator characteristics.

Table 5-2 Elevator Characteristics

Elevator Area	31 in^2
$Cm\delta_e$	-0.5042 rad^{-1}
$Cl\delta_e$	0 .1984 rad^{-1}
δ_{trim} (forward c.g.)	-0.8°
δ_{trim} (aft c.g.)	+2.7°
δ_{emax}	± 25°

5.2 Directional Stability and Control

The yaw moment coefficient can be broken down into two components, the component due to the yaw angle and that due to rudder deflection. The following are the governing equations for directional stability :

$$Cn = Cn_\beta \beta + Cn_{\delta_r} \delta_r$$

The directional stability derivative Cn_β can be resolved into two components,

$$Cn_\beta = Cn_{\beta_{wf}} + Cn_{\beta_v}$$

that due to the wing-fuselage, Reference [8] :

$$Cn_{\beta_{wf}} = -k_n k_{R_l} \frac{S_{fs}}{S_w} \frac{l_f}{b}$$

and that due to the vertical tail, Reference [8] :

$$Cn_{\beta_v} = V_v \eta_v C_{L_{\alpha_v}} \left(1 + \frac{d\sigma}{d\beta} \right)$$

The vertical volume ratio V_V used above is the following from Reference [8] :

$$V_V = \frac{l_v S_v}{S b}$$

That volume ratio was based on the wing span b, while the equation below was based on the chord, and the vertical tail aspect ratio is from Reference [7] :

$$V_V = \frac{l_v S_v}{S \bar{c}}$$

$$AR_v = 1.55 \frac{b_v^2}{S_v}$$

The maximum yaw angle β at trim conditions is equal to the following :

$$\beta_{trim_{max}} = \frac{- Cn_{\delta_r} \delta_{r_{max}}}{Cn_\beta}$$

5.2.1 Vertical Tail Sizing

The moment arm to the vertical tail, like that to the horizontal tail, is approximately a constant for a given c.g. location. From Reference [7], two rules of thumb were used. The first rule is that the vertical volume ratio (based on chord) equals 0.22 and second the aspect ratio should be between 2.25 and 3. This gave a vertical tail area of 86.25 in^2. We varied the aspect ratio to examine the span and chord variations. We again decided on a 7.5 inch chord, so this gave a 11.5 inch span. The span is defined as the distance from the top of the fuselage to the top of the vertical tail.

5.2.2 Rudder Sizing

Again a rule of thumb was used from Reference [7]. This rule is to have a rudder area to vertical tail area of approximately 0.3 to 0.4. We decided to size

the rudder at 40% of the vertical tail area to insure that we have enough rudder power to induce the yaw angle necessary to roll. The following equation is used to determine the rudder control power, Reference [8] :

$$Cn_{\delta_r} = - \eta_v V_v C_{L_{\alpha_v}} \tau$$

Table 5-3 shows the characteristics of the vertical tail and rudder.

Table 5-3 Vertical Tail and Rudder Characteristics

Moment Arm	31.1 in
Aspect ratio	2.38
Chord	7.5 in
Span	11.5 in
Planform Area	86.25 in^2
$Cn_{\beta wf}$	-0.004 rad^{-1}
$Cn_{\beta v}$	0.116 rad^{-1}
Cn_{β}	0.111 rad^{-1}
$Cn_{\delta r}$	-0.066 rad^{-1}
Rudder Planform Area	34.5 in^2
$\delta_{r\ max}$	± 30°
$\beta_{max\ trim}$	± 17.9°

Figure 5-9 shows the yaw moment coefficient as a function of yaw angle and rudder deflection.

5.3 Roll Stability and Control

We opted in our design to use the combination of yaw and wing dihedral to induce the required amount of roll. The decision was made to use this instead of ailerons because of the weight that an aileron control system would add. However, a small disadvantage is that a slightly larger vertical tail and rudder is needed compared to an aircraft with ailerons. Since our design is a high wing with a positive dihedral angle, the aircraft will possess roll stability. The following are the governing equations for roll and the

change in angle of attack as functions of the sideslip (or yaw) angle and dihedral angle:

$$C_l = \frac{C_{l_\beta}}{\Gamma} (\Gamma \beta)$$

where the term $\frac{Cl_\beta}{\Gamma}$ is determined from Figure 3.9 in Reference [8] to be equal to -0.00024.

$$\Delta\alpha = \tan^{-1} (\sin \beta \tan \Gamma)$$

Figure 5-9 Cn vs Yaw Angle

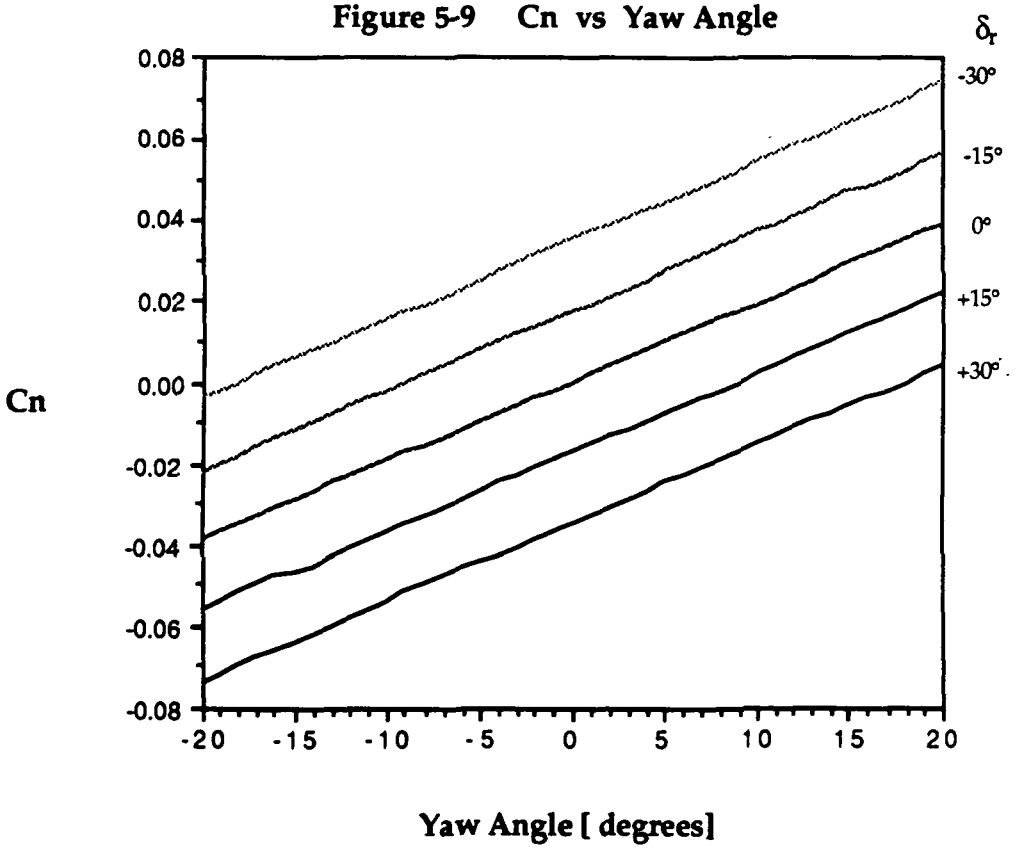

5.3.1 Wing Dihedral

There is loss of lift due to dihedral, so it is desired to keep the angle small. From References [7] and [4], it was determined that the range in desired dihedral angles was from 5° to 10°. At these angles only a very small percentage of the lift is lost. Because of this we decided that a "V" type dihedral would be used since other types are only slightly more efficient, while being more difficult to construct. Also other types of dihedral would have increased the structural weight of the wing.

The roll moment coefficient is plotted in Figure 5-10 as a function of both yaw angle, (which is also the sideslip angle, β) and dihedral angle. Since the rudder has already been sized, the constraint on the yaw angle is known to be approximately $\pm$ 18°. The rudder deflection creates a yaw angle which, with the wing dihedral, induces roll through a small change in angle of attack. From Reference [4], the estimated roll moment coefficient required to satisfy the turning requirement is approximately 0.031. Therefore we decided upon a dihedral angle of 9°. Figure 5-11 shows the change in angle of attack associated with the yaw and dihedral angles. The maximum $\Delta\alpha$ is approximately 2.8°.

5.4 Final Remarks

The aircraft is both longitudinally and laterally statically stable. However, it is not too statically stable, which would impair maneuverability. There is also sufficient control power to maneuver the aircraft.

Figure 5-10 Cl vs Yaw Angle

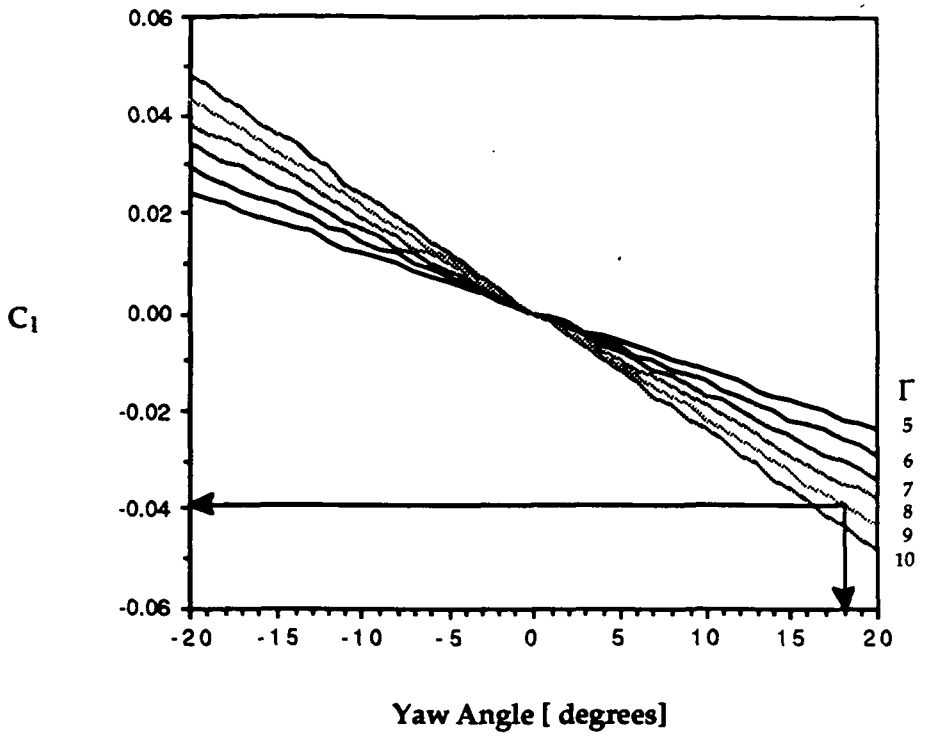

Figure 5-11 Change in Angle of Attack vs Yaw Angle

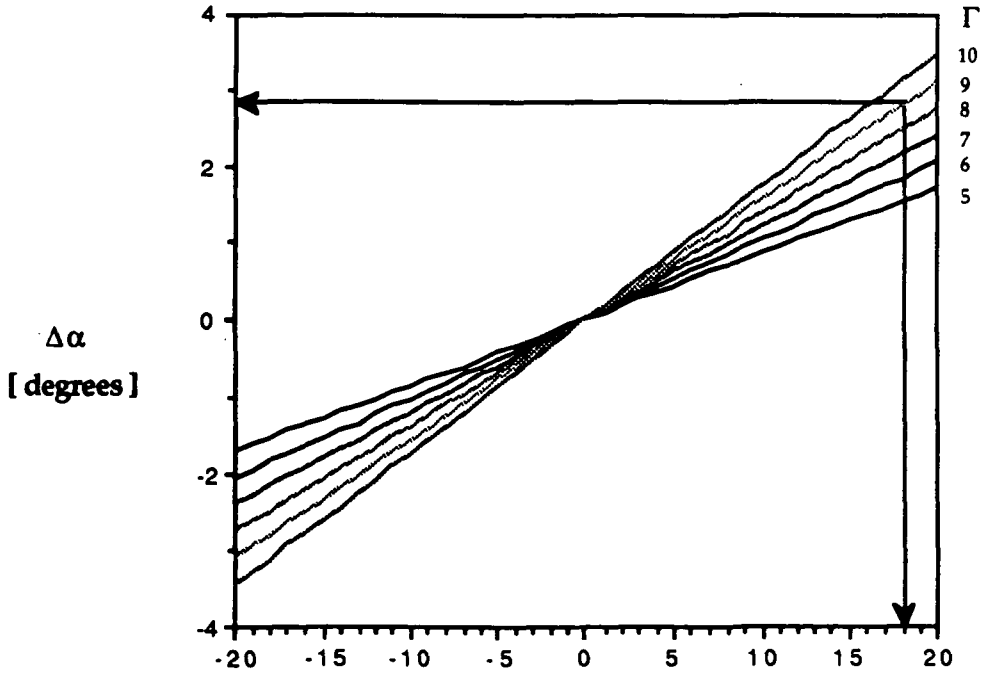

6. STRUCTURES

6.1 V-n Diagram

Before any structural analysis can be started, it is important to know the load range that the aircraft will be operating in during flight. The V-n Diagram for our aircraft can be seen in Figure 6-1 below.

Figure 6-1: V-n Diagram

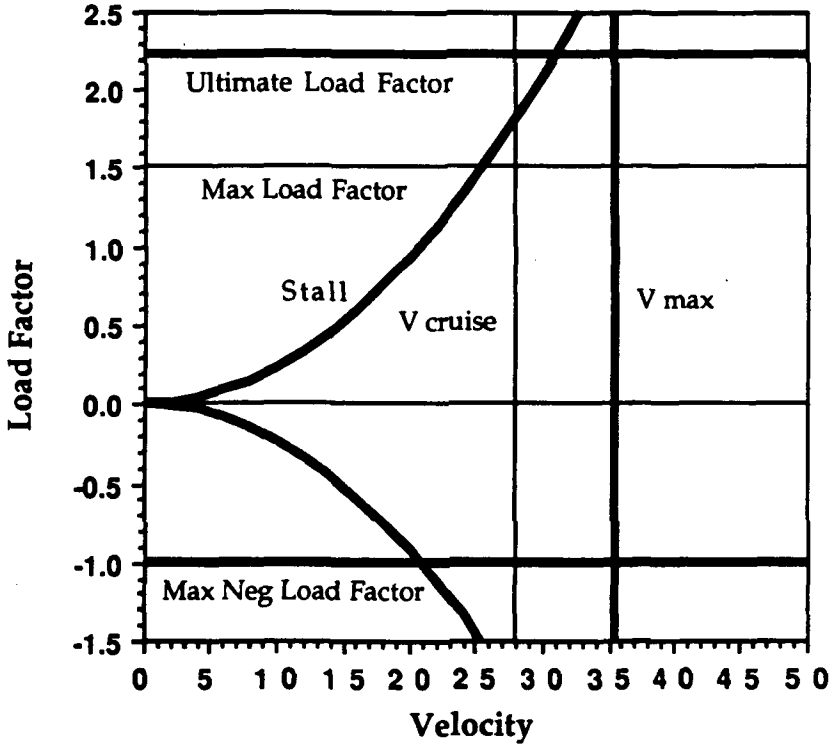

Wind gusts were not included because our test aircraft will be flown inside where no gusts will be encountered. The maximum load factor of 1.5 was based on a banked 60 ft radius turn, and the ultimate load factor of 2.25 includes a factor of safety of 1.5. Our minimum velocity is 21 ft/s, our maximum velocity is 35 ft/s, and our cruise velocity is 28 ft/s. An important

point to note about Figure 6-1 is that by designing our aircraft to these specifications, the aircraft will stall before it reaches structural failure when operating at the cruise velocity. This is a good result due to the limited predictability of the aircraft's response characteristics during initial flight tests.

6.2 Materials Selection

When selecting the materials that the aircraft would be constructed from, the following characteristics were considered: strength, weight, cost, availability, and machineability. Due to our limited budget, cost became an overriding factor. Out of the possible choices: wood, metals, ceramics, or composites, wood is definitely the least expensive. In terms of availability and machineability, it also rates highest among the other materials. The strength and weight of wood may not be as good as the other materials, but for our design, they should be sufficient to accomplish our mission. Thus, we selected wood as the primary material from which we will construct our aircraft. In order to create a skin surface for our aircraft, we decided to use a monokote type skin which is light and, also, relatively simple to construct.

Another advantage to choosing wood as our primary material is the various types of wood that are available. The various types have various maximum allowable stresses associated with them, which allows us to keep the aircraft's weight as low as possible by using only high strength wood in high stress areas. Table 6-1, shown below, lists the types of wood that will be used in our aircraft with their corresponding densities and allowable stresses.

Table 6-1: Material Summary

Wood	Density (lb/in^3)	Max Allowable Stress (psi)
Balsa	0.0058	400
Spruce	0.0160	6200
Birch Plywood	0.0230	2500

6.3 Structural Components

6.3.1 Wing

The structural integrity of the wing is a critical design consideration for our aircraft. The key design objective is that the wing will not fail under maximum load conditions. These conditions can be estimated to be the greatest when the plane is in its banked, minimum radius turn. When under these maximum conditions, a failure criteria must be established, and the most logical one is that failure will occur at the root of the main spar due to axial stress from bending. The assumption here is that the spars in the wing will carry all the load (the ribs will not carry any load, but will only help retain the shape of the wing), and the wing can therefore be modeled as a cantilevered beam. The following analysis was based on this model.

Using the above model for the wing, it is obvious that the key parameters that can be controlled have to do with the spars. The number of spars, the dimensions of the spar caps, the percent thickness of the airfoil, and the type of material used for the spars are all key parameters that can be controlled and varied to determine their sensitivity to the maximum allowable stress in the wing. By determining the maximum stresses in the wing with these parameters, the limits on these parameters that must be met in order to avoid wing failure can be found. This, therefore, makes the wing strength a figure of merit for this analysis. How low of an axial stress that exists in the wing is an excellent measure of the structural integrity of the wing. Another figure of merit would be the wing weight. Obviously, the lighter the wing, the better the aircraft will perform. The design of a wing that is both light and strong was, of course, the optimal solution. Some constraints that must be considered include the following: the maximum allowable stress levels for certain materials, upper limits on the wing weight, and the size of the wing. The following analysis was performed using all of the above parameters.

To model the point of maximum stresses, a fully banked, minimum radius turn was considered under the same conditions as described for the V-n Diagram in Figure 6-1. Using this maximum loading condition, the

maximum stresses were calculated. The stresses were calculated using the following formula:

$$S_{xx} = \frac{-M_z\, y}{I_{zz}} + \frac{M_y\, z}{I_{yy}} \qquad (1)$$

This formula allows for the inclusion of both the lift and drag forces that the airfoil would encounter. These forces were considered to act at the midpoints of the wing in order to simplify the calculation of the moments. By choosing spruce wood as the material for the spar caps, the wing can sustain a maximum allowable stress of 6200 psi. Including a factor of safety of 2, this reduces the allowable stress to 3100 psi. The above model was used for the wing analysis, and the analysis was performed using TKSolver Plus. All variables and equations can be seen in Appendix D-1. Although the ribs are not considered to add to the strength of the wing, they were included to help compute the total weight of the wing.

Initially, we looked at the effect of the number of spars on the axial strength of the wing in order to eliminate this variable early. Quick calculations showed that one main spar positioned at the maximum thickness point in the airfoil was more than strong enough to withstand maximum stresses that would be encountered during flight. This also allows for the wing weight to be kept low which is a figure of merit. Next, we looked at the effect that the spar cap dimensions had on the axial stresses in the wing keeping the wing dimensions constant. The results of this analysis can be seen in Figure 6-2.

Figure 6-2: Axial Stress vs. Height of Spar Cap: Lines of Constant Spar Cap Width

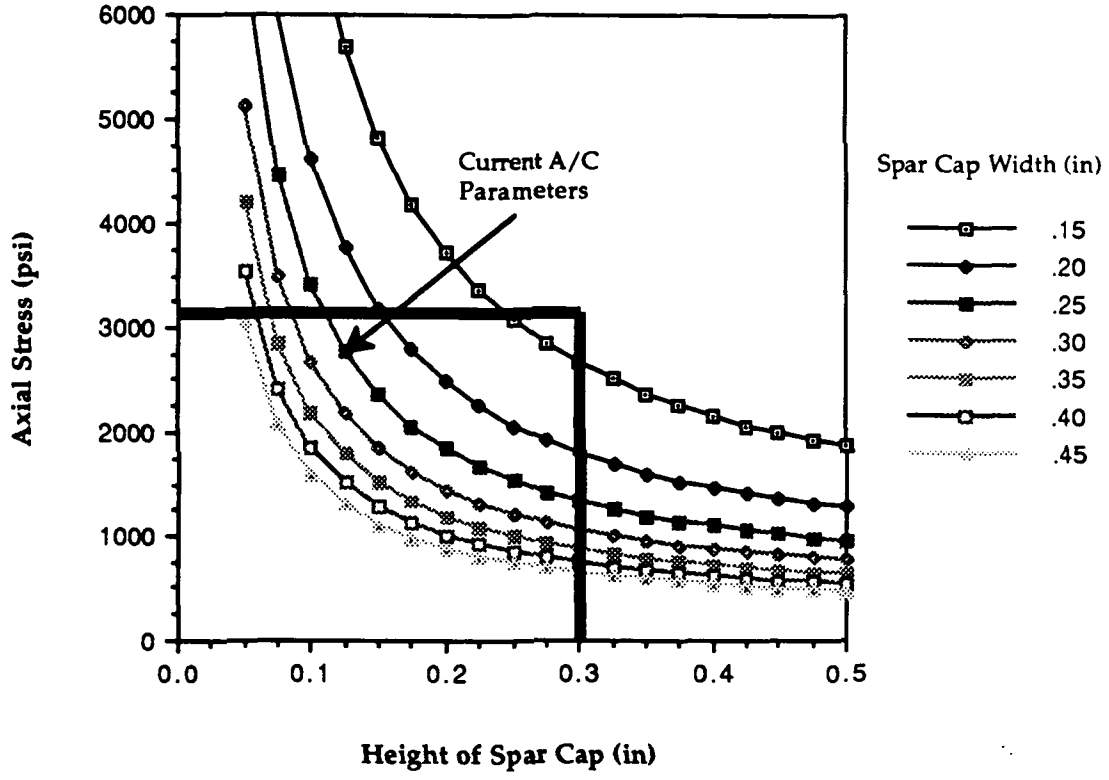

From Figure 6-2, a number of trends can be determined. First, as the area of the spar cap increases the axial stress in the spar cap decreases as expected. More specifically, though, further changes in the height of the spar cap over 0.3 inches has little effect in lowering the axial stress. Thus a constraint was placed on the height of the spar cap. The upper constraint coincides with the 3100 psi upper limit on the maximum allowable stress discussed earlier. A similar trend can be noticed with the width of the spar cap. After a width of 0.3 inches is reached, the effect of further widening the spar cap results in small reductions in the axial stress. With these upper limits in mind, it was next beneficial to look at what combinations would provide an optimum weight for the wing.

The next part of the analysis involved studying what effects the spar cap dimensions had on the wing weight for various stress levels, once again, keeping the wing dimensions constant. The results of this analysis can be seen in Figure 6-3.

Figure 6-3: Wing Weight vs. Spar Cap Height: Lines of Constant Axial Stress

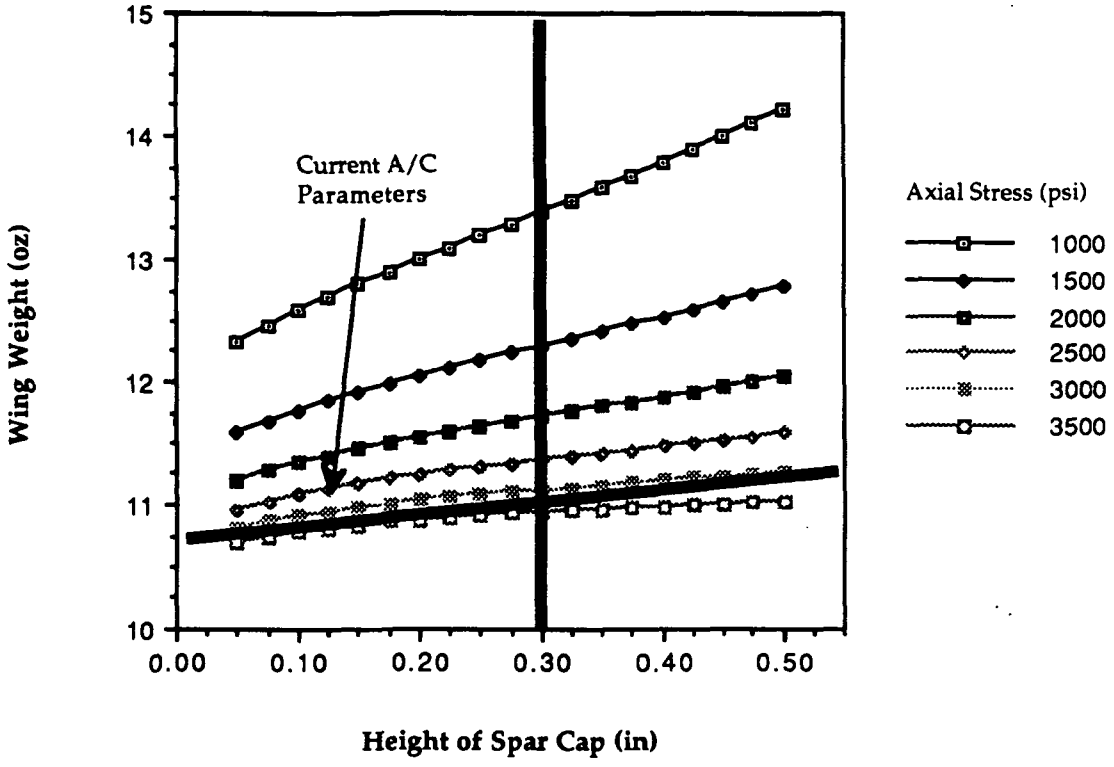

From this figure, a number of trends can be determined. First of all, the constraints that appear in this figure are the same that appeared in Figure 6-2, a maximum spar cap height of 0.3 in and a maximum allowable stress of 3100 psi. One can immediately see that in order to maintain low stress levels, high penalties in wing weight are taken. On the other hand, increases in the stress level, allows for lower ranges of wing weights to exist. In addition to this, however, increases in the stress level causes variations in the spar cap height to have little effect on the wing weight. This could be a desirable effect because at these stress levels, design changes requiring increases in the spar

cap height would pay a small price in the wing weight. These previous studies help to determine the optimum spar cap dimensions for a specific wing, but it would be important to look at what effect varying the wing dimensions would have on the stress level for constant spar cap dimensions.

The final part of this analysis focused on studying the effect of varying all the wing dimensions (surface area, span, chord, aspect ratio, and wing weight) on the axial stress level in the wing. The results of all these calculations can be seen in a carpet plot shown in Figure 6-4.

Figure 6-4: Axial Stress vs. Surface Area of Wing: Lines of Constant Wing Dimensions

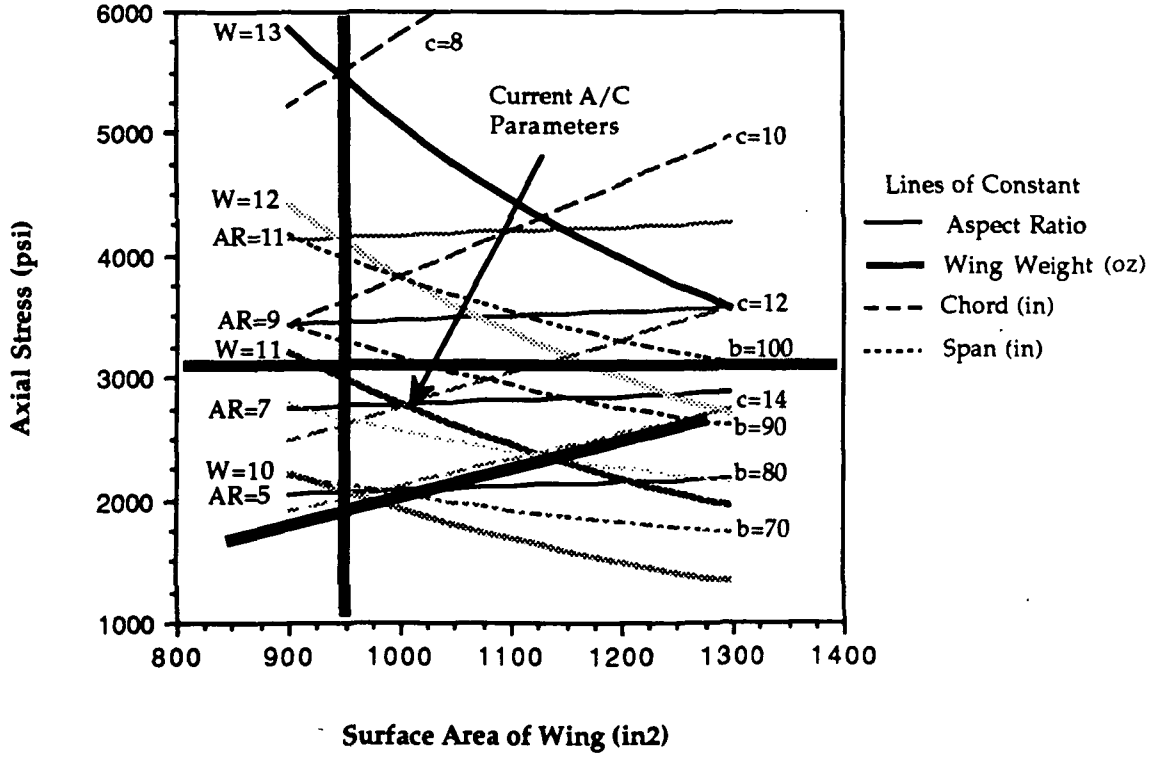

From this figure, a number of trends can be interpreted. Looking at the effect of varying the surface area of the wing holding the aspect ratio constant, one can immediately see that it had negligible effect on the axial stress. The lines are practically flat. On the other hand, varying the surface area of the wing

holding the wing chord constant had the largest effect on the axial stress. Increases in the surface area resulted in large changes in the axial stress. Also, decreases in the chord length greatly increased the stress level in the wing. Variations in the surface area with a constant wing span showed a small effect on the axial stress. The most interesting effect, however, involved the variation of the surface area holding the wing weight constant. While keeping the wing weight constant, increases in the surface area of the wing actually lowered the stress level in the wing. This is a very encouraging result, because if design changes required more wing surface area, it could be possible to redesign the wing for the same weight and not have to worry about increasing the stress levels in the wing.

Using the results of this analysis, the current design of the internal structure of the wing was determined and can be seen in each figure indicated by the current aircraft parameters arrow. For clarity, they are also listed in Table 6-2 below.

Table 6-2: Summary of Aircraft Wing Parameters

Wing Dimensions		Internal Wing	
Aspect Ratio	7	Spar Cap Height	0.125 in
Span	84 in	Spar Cap Width	0.250 in
Chord	12 in	Wing Weight	10.0 oz
Surface Area	1008 in^2	Max Axial Stress	2772 psi
Thickness	1.8 in		

6.3.2 Fuselage

When sizing our fuselage, the main parameters that were considered were that there was enough room to carry our design payload, and the size of our tail moment arm. The fuselage overall length is 51 in, which is a sufficient distance to mount our wing and have enough of a tail moment arm to keep our tail size down. The fuselage is also made up of primarily square cross sections with the maximum size being 5 in by 5 in. This type of cross section

not only allows for simpler construction, but also provides ample space to carry our design payload goal.

Considering that wood was chosen as our primary material for construction, we decided that a truss structure would be the best option for building our fuselage. The actual truss structure can be seen in Figure 6-5. Most of the structure will be made out of balsa wood along with some birch plywood that will be used for planking. Our design was based primarily on previous designs and the study of RPV expert, Mr. Joe Mergen's designs. Due to the complexity of the structure, the fuselage was simplified so that simple beam theory, as discussed in the wing design, was used to verify its structural integrity.

6.3.3 Empennage

The internal layout of the tail section of our aircraft was designed primarily the same way as the fuselage was designed. The tail is made of a truss configuration using balsa wood as the material for the members. The actual truss configuration can be seen in Figure 6-6. The sizing of the tail was based primarily on stability and control considerations, but the internal design was based primarily on keeping the weight of the tail low. This is because the tail has a large moment arm, and its weight has a large effect on the center of gravity position for the aircraft.

6.3.4 Landing Gear

There were a number of considerations that we looked at when we were designing our landing gear. The first consideration was ground handling, and after consultation with Mr. Mergen we opted for a tail dragger configuration over a tricycle landing gear, because of the better handling qualities gained with a tail dragger. Also, the rear gear will be attached to the rudder to provide additional directional control on the ground.

Another main concern was the height of the landing gear. A minimum height was needed so that there would be enough ground clearance for the propeller, but a maximum height could not be exceeded so that the sitting angle of the plane would not have the wing in a stall position. Figure 6-7 shows the landing gear configuration for our aircraft. At the current design, our aircraft has enough ground clearance for a 12 in diameter propeller, and the combination of our sitting angle along with the mounted wing incidence has our wing at 8 degrees which corresponds to the maximum lift coefficient point. Finally, the choice of a 2 in diameter wheel is based on the rough surface conditions that will be encountered during testing and previous designs.

Figure 6-5: Truss Structure of Fuselage

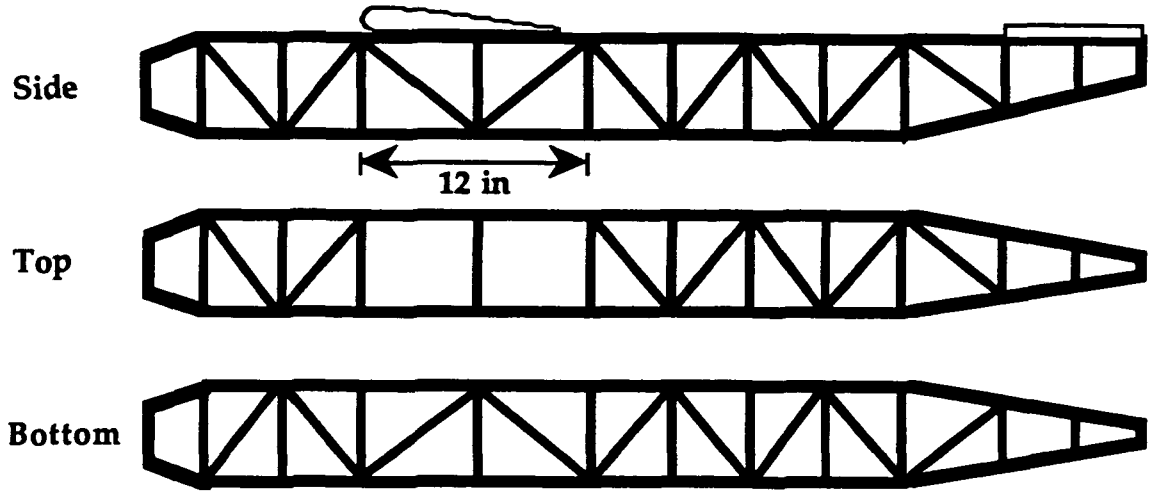

Figure 6-6: Truss Structure of Empennage

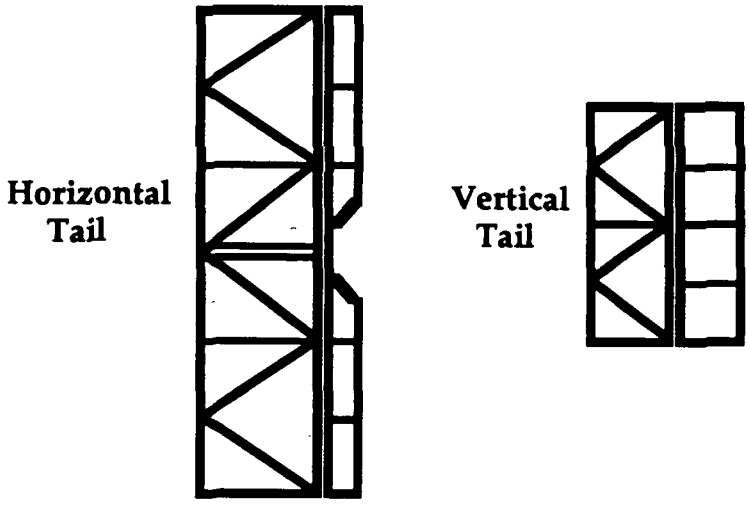

Figure 6-7: Landing Gear Configuration

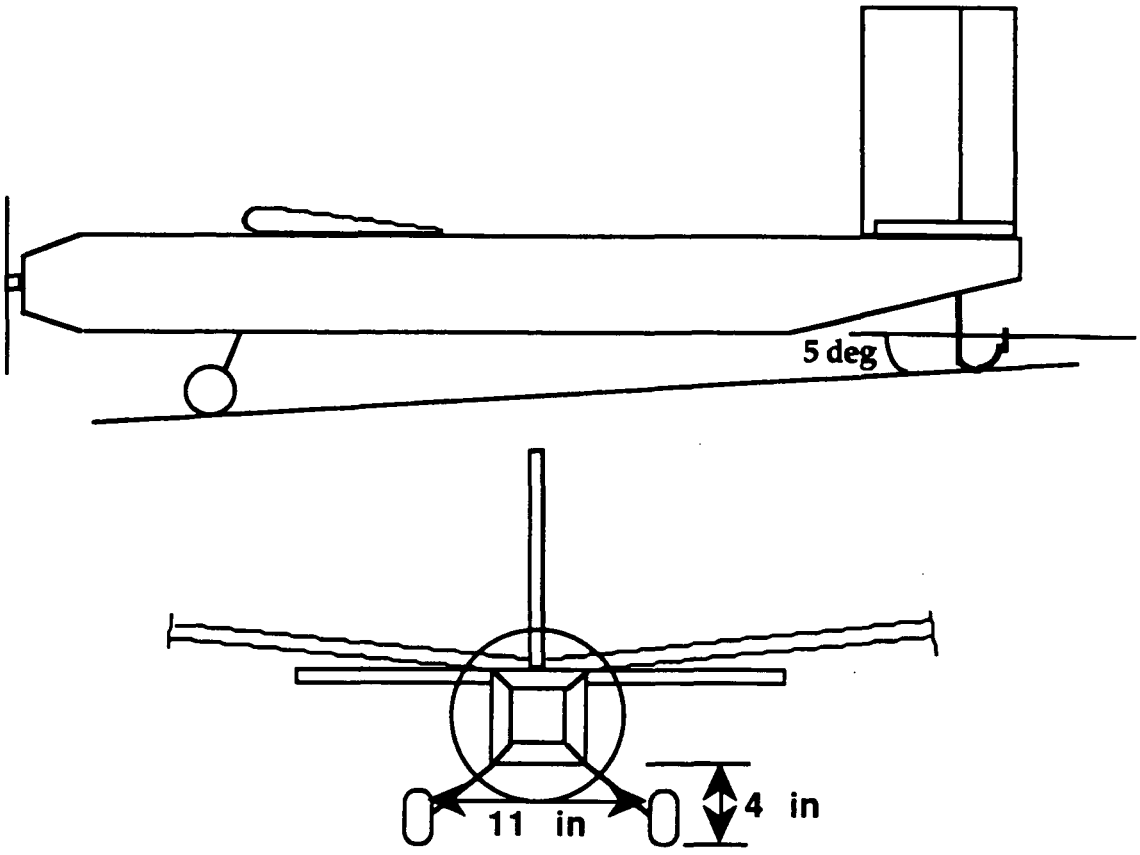

7. PERFORMANCE

7.1 Take-off and Landing

The basic constraints on take-off and landing performance of "The Initial Guess" were the characteristics of the airports it is designed to serve. A requirement of the mission evaluation is service to City B which has a shorter runway than other cities the transport will serve. Therefore, the maximum take-off and landing distances were constrained to 60 ft.

Take-off performance was examined for the extreme conditions of a transport with and without passengers. This was accomplished by doing an iteration to find the velocity and ground roll until the lift equalled the weight of the craft. (See Appendix E1.) The plane, full of passengers, has a ground roll distance of 44.7 ft and a take-off velocity of 27.4 ft/s. As expected, this is longer than the take-off distance for the empty craft which is 36.6 ft with a lift-off velocity of 26.3 ft/s. Each of these distances is sufficiently less than the 60 ft. maximum to allow for a significant safety factor.

Initial calculations of the landing distance indicated that the plane would not be able to stop on the 60 ft. runway at City B. However, these calculations use a minimum glide angle, do not take any elevator deflection into account, and neglect the effect of flare during descent. The flare of the craft will significantly reduce landing distance by increasing drag and thus slow the craft down.

Ground effects were also examined as a possible factor in the design. A program was written to determine what effects the height of the wing off the ground (a variable in ground effect calculations) would have on take-off distance. (See Appendix E2.) The effects were found to be so minimal that the design was not influenced.

7.2 Cruise

Cruise performance was determined with minimum current draw from the motor at both full and empty passenger configurations. This is due to our overall mission objective of maximizing profits. Minimizing fuel consumption, i.e. current draw, is the primary way to keep operating costs down.

A full aircraft draws 3.33 Amps during cruise which translates to a maximum range of 12,107 ft. and an endurance of 7.21 min. When empty, the transport will draw 3.06 Amps during cruise, have a range of 13,186 ft., and have an endurance of 7.85 min. These values represent the maximum possible ranges and endurances. Taking into account the time spent on the ground with the motor running (taxiing to and from the gates, waiting in line to be cleared for take-off), time which may be spent loitering above the destination city waiting to land, and a factor of safety, the range of the craft with a full passenger load is estimated to be at the design range of 5500 ft. The empty transport will have a slightly longer range.

The range of the transport was plotted versus the payload. (See Figure 7-1.) This figure shows the trend of decreasing range with increasing payload. However, the rate of decrease is small, therefore, carrying a larger number of passengers is not a large detriment to the overall design, and the added income of these passengers is needed to maximize profits. One aspect of the larger payload which is quite detrimental is the added volume necessary to accommodate the extra passengers. Increasing the number of passengers significantly increases the required size of the fuselage which will add drag and weight and may add blockage of the propeller (if the cross-sectional area is increased). A possible derivative design from this transport would be a cargo-carrying aircraft which would be able to take advantage of all of the volume on the plane without concern for the comfort of the payload (i.e., no aisles, lavatories, etc.).

Figure 7-1
Range vs Payload

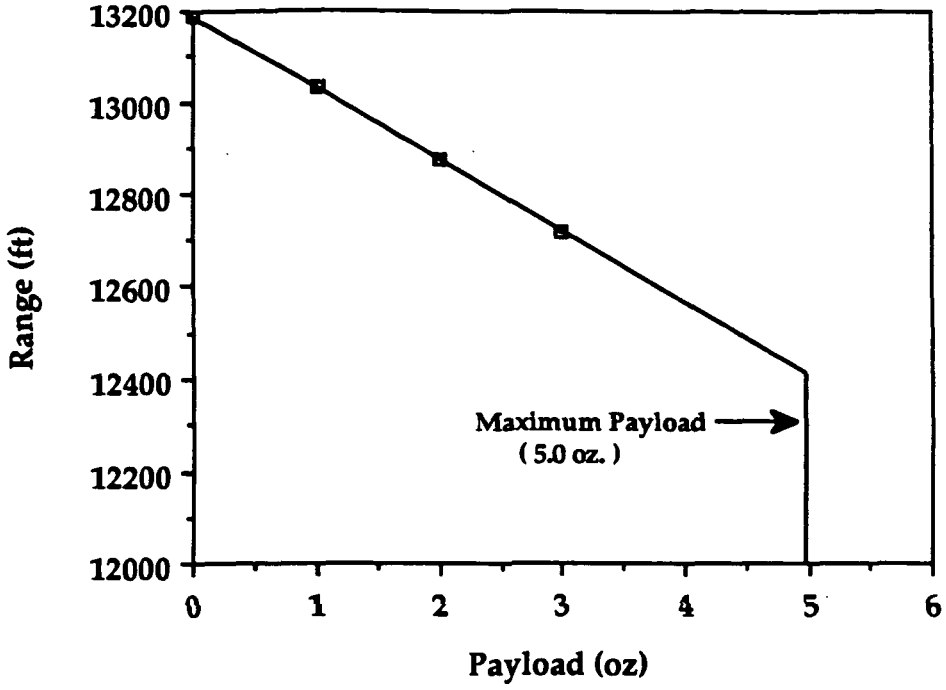

The power available versus power required curve (See Figure 7-2.) allows the calculation of the rate of climb.

$$\text{Rate of Climb} = \frac{P_{avail} - P_{req}}{W}$$

At cruise velocity, the rate of climb is approximately 14 ft/s.

7.3 Turning Flight

The maximum turn radius allowed for the aircraft was determined by the conditions of the flight test it will have to pass. The transport will be tested in an enclosed area such that the maximum turn radius is restricted to 60 ft. The necessary Cl required for maintaining a steady, level, banked turn at V = 28 ft/s was investigated using calculations on a spreadsheet. (See Appendix E3.)

Figure 7-2
Power Available vs. Power Required
Motor: Astro 05
Propeller: Zinger 10-6

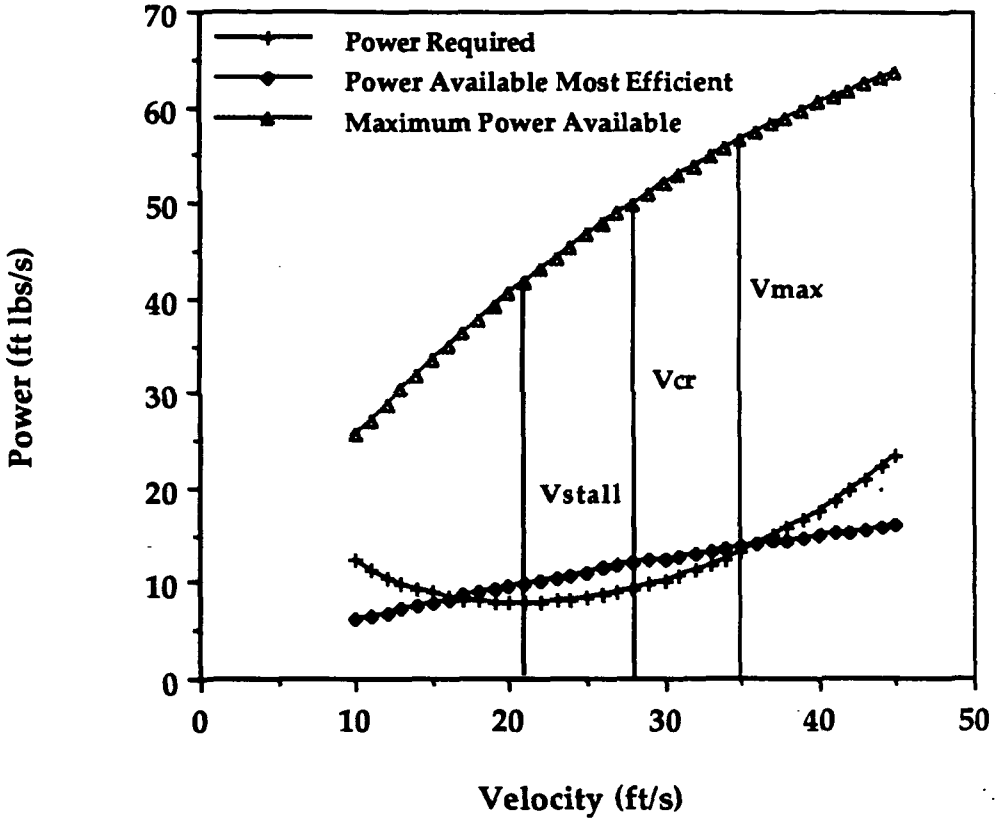

The turn radius was determined from the cruise velocity, lift, and weight. [2]

$$R = \frac{V^2}{g\,(n^2 - 1)^{1/2}}$$

The aircraft will meet the turn radius requirement with a lift coefficient of 0.63 or greater at a bank angle of 18.7°. The incidence angle of the wing is 3°, and the aircraft is designed to fly level, so the coefficient of lift during cruise will be 0.71. This corresponds to a turning radius of 31.2 ft which is well within the objective radius of 60 ft.

Table 7-1: Performance Characteristics

Payload Capacity	Full	Empty
Weight	58 oz.	53 oz.
Take-off Performance:		
Ground Roll Distance	44.7 ft.	36.6 ft.
Time to Take-off	3.2 s	2.8s
Take-off Velocity	27.4 ft/s	26.3 ft/s
Cruise Performance:		
Cruise Velocity	28 ft/s	
Current Draw	3.33 amps	3.06 amps
Range	12,110 ft	13,190 ft
Endurance	7.21 min	7.85 min
Turn Radius	31.3 ft	
Maximum Rate of Climb	14 ft/s	

8. MANUFACTURING/PRODUCTION COST

8.1 Production Cost

The production cost analysis which was completed for our aircraft was broken down into two parts: materials and labor. The cost (in AEROWORLD dollars) for materials includes a radio system at $46,400, a motor at $36,400, two servos for a total of $26,400, a speed controller for $40,000, and wood, monokote, and additional expenses totalling $80,000. While the first four items are somewhat controlled costs and rather accurate (because they will be supplied by the manufacturer for the said price), the price for wood, monocote, and other parts represents an educated guess based on past years projects as well as the amount of money which was allotted to us for production. Because of this, the value listed for wood and monocote may very well wind up changing. As of now, however, the cost for materials is set at $229,200.

The cost for labor is also somewhat of an estimate. It was found that for 7 employees working for 3 weeks while spending 8 hours per week working, a total of 168 production hours would be accumulated during the production of the aircraft. This time period is based on the amount of time which we considered to be reasonable. At the going rate of labor of $100/hour, the labor cost for this time is calculated to be $16,800. This sets the total cost of production at $246,000. While this is an educated guess, it is what we feel to be an accurate one.

8.2 Ticket Pricing Analysis

It is highly important in the Aeroworld airline industry, as it is in any business, to make a profit. For this reason, airplane ticket prices should be high enough to allow an airline to yield a worthwhile profit, yet low enough to remain competitive with both other airlines and other means of transportation. By setting our ticket prices at $12/50 ft in addition to a $75 flat fee per person, Kappa Aerospace is fulfilling these requirements.

Figure 8-1 below shows a graph of ticket revenue and operational cost vs. range. In the graph, the two solid lines represent operational costs for the high and low range of fuel cost in Aeroworld. These costs also reflect a $500 maintenance fee per flight and a $200 fee for a crew and stewardess. The other symbols on the graph represent ticket revenue based on a full plane of 56 passengers. It can be seen that for a price (per person) of approximately $10.20/50 ft + a $75 flat fee, our airplane will break even. Any additional revenue above this ticket price will result in profit. Therefore, in order to make an acceptable profit while remaining competitive, we chose to set our ticket prices at $12/50 ft in addition to a $75 flat fee.

Figure 8-1

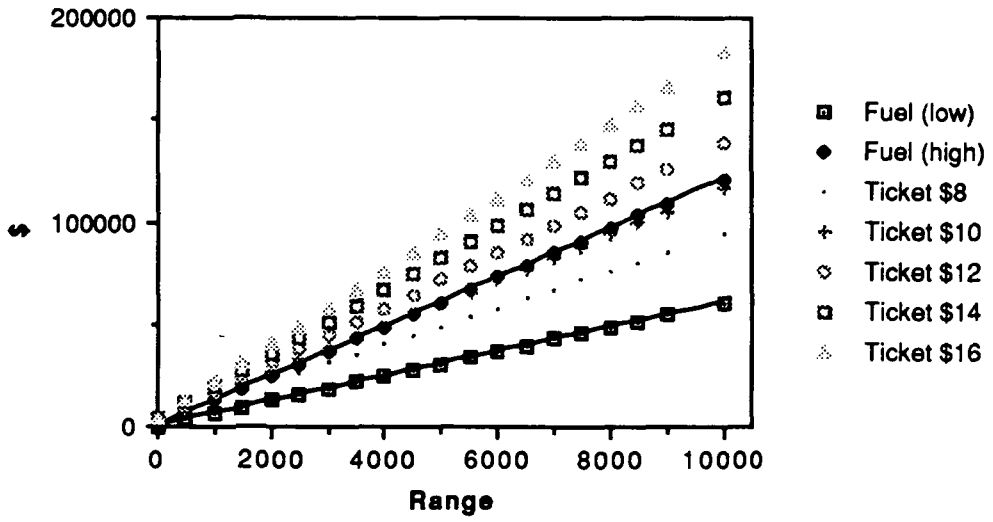

In comparison to other means of travel within Aeroworld, our ticket prices are extremely competitive, especially given the many benefits of air travel. An example of this can be seen by looking at travel between cities K and L. Travelling by boat would cost over $422 while air fare can be purchased for $611. Likewise, between cities L and M train fare is $300 while air fare is only $555. In both cases, the fare charged to fly is reasonable in comparison to other means. Another point that should be noted is that at our given ticket price the profit made on an average flight of 2500 ft while carrying 56 passengers is over $5000. With the cost of production estimated at $246,000, the payoff time for our aircraft is just 49 flights. Every flight after that would result in pure profit for the company.

9. TECHNOLOGY DEMONSTRATOR

9.1 Construction

In order to demonstrate the predicted performance of our aircraft, we built a model of our aircraft, a technology demonstrator. This model was constructed in a three week period according to our design proposal. Due to the inexperience of all our members with the building of RPVs, many lessons were learned. This section will summarize our findings during the construction of our aircraft.

We began the construction of our aircraft by building the framework for the fuselage, empennage, and the wing. We quickly learned that the dimensions of the wood that we were using to build our frame structure were larger than needed, but rather than risk safety, we decided to continue following the proposal. After the framework was completed, we began adding the internal components and connecting the control surfaces to the servos. Our internal layout differed from our planned internal layout due to missed considerations involving wiring and control linkage lengths. We were, however, able to adapt and overcome this new problem. Finally, we monokoted all the framed pieces and attached the landing gear. When we monokoted our wing, we did not realize that the shrinking monokote could twist our wing. We were able to correct this problem by twisting the wing in the opposite direction and reshrinking the monokote to hold the wing true.

One of our main goals, and challenges, when constructing our aircraft was to remain within the weight ranges for the components of our aircraft so that our center of gravity will remain at the predicted point. Table 9-1 shows the predicted versus actual weights for our aircraft along with the predicted and actual center of gravity positions.

Table 9-1

Component	Weight Predicted(oz)	Weight Actual (oz)
Propeller	1.00	1.00
Engine	6.50	6.50
Engine Mount	1.14	1.14
Batteries (Eng.)	6.24	14.00
Batteries (Sys.)	2.00	2.00
Receiver	0.95	0.95
Servos	1.20	1.20
Speed Controller	3.23	3.23
Wing	10.00	10.35
Fuselage	11.80	11.04
Empennage	5.00	2.91
Landing Gear	7.00	6.50
Payload	4.94	4.94
Total	**61.00**	**65.76**
X/c (c.g.)	0.32 (Predicted)	0.33 (Actual)

All the weights are very close to their predicted values, except for the battery weight. Due to the unavailability of the size battery that we wanted and the need for a higher voltage, we had to use more batteries than predicted which tremendously increased our battery weight. This results in the higher total weight for the aircraft. We were still able to keep the center of gravity in the same position because the placement of our batteries is variable. In order to test our aircraft, however, we will not fly with full payload which will allow us to bring the weight of our aircraft down to its designed weight.

9.2 Flight Testing

In order to validate our technical demonstrator, observe any correctable shortcomings, and make necessary corrections before the actual flight testing

on Friday May 3, 1991, two days of pre-flight tests were scheduled to be conducted on the preceding Tuesday and Thursday.

On the Tuesday preceding, plans for testing *"The Initial Guess"* included several taxi tests, a test of the control surfaces, and a simulated take-off. The taxi tests will allow the ground handling qualities of the airplane to be observed and corrected if need be. By testing the control surfaces we will be avoiding any potential problems which may otherwise prevent the aircraft from flying successfully on Friday. The culmination of these activities will occur with the simulated take off. This will allow both ground handling and control surfaces to be tested simultaneously. In addition to these dynamic tests, the location of the aircraft's center of gravity will be examined, so that it may be corrected if it is in the wrong place.

The corrections which will be made following Tuesday's test will be examined on Thursday. This will include more taxi tests as well as a longer simulated take off. Although the aircraft will not perform any maneuvers during this simulation, it will fly for a greater distance than on Tuesday. Corrections will be made for any shortcomings and the center of gravity will once again be checked. These tests will be critical to the success of the aircraft in that they will be the last opportunity to observe any potential problems.

On Friday the final flight test will be conducted. This is will be the ultimate test of the aircraft, and thus all corrections made must be final at this time. This includes having acceptable ground handling qualities and the required center of gravity location in order to ensure stability. The flight test itself will occur in the Loftus Indoor Sports Complex and will consist of a take off from a designated area, several figure eight maneuvers, and a landing. In order to document the flight speed, several team members will be located around the field with stopwatches. The observed velocity will be compared to the design cruise velocity. Also it should be noted that an experienced RPV pilot will be flying the aircraft.

Appendix A: Performance Spread Sheet

To evaluate the performance of various motor/propeller combinations, a spread sheet was developed to calculate power available, power required, and current draw. The relevant aircraft parameters (weight, aspect ratio, planform area, etc.) were to be input such that they could be changed without causing extensive reediting of the spread sheet. This goal was accomplished by making the top portion of the sheet the input section for the aircraft's parameters, and all subsequent calculations based on the spaces reserved for these parameters. The sample spread sheet provided shows the current status of our aircraft when operating at full capacity. The motor characteristics required and the equations used for the calculations are listed below. The current draw during cruise can be obtained by interpolating the values to 0 rate of climb.

Given in motor performance sheet: Gear RPM, Gear Power, and Battery Volts

Equations used for Calculations:

Advance Ratio: $$J = \frac{V}{nD_{Prop}}$$

Propeller Efficiency: $\eta = \eta(J)$ Dependent upon which propeller used

Power Available: $$P_a = \eta * \text{Gear Power} * 0.737 \frac{\text{ft lb/s}}{\text{watts}} * 60\%$$
(note: 60% factor to compensate for blockage.)

Power Required: $$P_r = \left(C_{d,o} + \frac{C_L^2}{\pi e AR} \right) * 0.5 * \rho * S * V^3$$

Rate of Climb: $$R/C = \frac{P_a - P_r}{W}$$

Current Draw: $$I_a = \frac{V_{bat\ oc} - E}{R_{bat} + R_{motor}}$$

Amp-Hr usage: $$\text{AmpHr} = \frac{\text{Range} * I_a}{V} * \frac{1\ hr}{3600\ s}$$

Performance Spread Sheet: Astro O5 with Zinger 10-6

Motor	Propeller								
Astro 05	Z10-6								
density	Q (lb/ft^2)	Tot wt (lbs)	Diameter (in)	Vcr (ft/s)	Cd,o	S (ft^2)	aspect ratio	Oswald e	Cl cruise
2.25E-03	0.88	3.563	10.0	28.0	0.0288	7.0	7.0	0.7	0.6

Kv (V/RPM)	Vbat,oc	Rbat	BtCap amphr	Range (ft)
3.38E-04	8.930	0.050	0.800	5500.0

Calculations			W	ft lb/s	ft lb/s	ft/s		Amps		
Gear RPM	J	Prop effic	Gear Power	Power Avail	Power Req	R/C	AmpHr draw	Current draw	E (volts)	Motor Ohms
10788.0	0.187	0.469	0.0	0.00	8.72	-2.45	0.05	0.9	8.84	0.05
10302.0	0.196	0.484	32.8	7.02	8.72	-0.48	0.15	2.8	8.65	0.05
10179.0	0.198	0.487	40.3	8.69	8.72	-0.01	0.17	3.2	8.61	0.05
10055.0	0.200	0.491	47.7	10.37	8.72	0.46	0.20	3.7	8.56	0.05
9929.0	0.203	0.495	54.8	12.01	8.72	0.92	0.22	4.1	8.52	0.05
9802.0	0.206	0.499	61.7	13.63	8.72	1.38	0.25	4.6	8.47	0.05
9674.0	0.208	0.504	68.4	15.24	8.72	1.83	0.28	5.1	8.42	0.05
9545.0	0.211	0.508	74.9	16.83	8.72	2.28	0.30	5.5	8.38	0.05
9414.0	0.214	0.512	81.2	18.41	8.72	2.72	0.33	6.0	8.33	0.05
9282.0	0.217	0.517	87.3	19.97	8.72	3.16	0.35	6.4	8.29	0.05
9148.0	0.220	0.522	93.1	21.49	8.72	3.59	0.38	6.9	8.24	0.05
9013.0	0.224	0.527	98.8	23.02	8.72	4.01	0.36	6.6	8.20	0.06
8876.0	0.227	0.532	104.2	24.51	8.72	4.43	0.39	7.1	8.15	0.06
8738.0	0.231	0.537	109.3	25.96	8.72	4.84	0.41	7.5	8.11	0.06
8598.0	0.234	0.542	114.3	27.43	8.72	5.25	0.43	7.9	8.06	0.06
8457.0	0.238	0.548	119.0	28.85	8.72	5.65	0.46	8.4	8.01	0.06
8314.0	0.242	0.554	123.4	30.23	8.72	6.04	0.48	8.7	7.97	0.06
8170.0	0.247	0.560	127.6	31.59	8.72	6.42	0.50	9.2	7.92	0.06
8024.0	0.251	0.566	131.6	32.94	8.72	6.80	0.52	9.5	7.88	0.06
7876.0	0.256	0.572	135.3	34.25	8.72	7.17	0.55	10.0	7.83	0.06
7727.0	0.261	0.579	138.7	35.51	8.72	7.52	0.57	10.4	7.79	0.06
7576.0	0.266	0.586	141.9	36.76	8.72	7.87	0.59	10.8	7.74	0.06

Appendix B.

The items listed in the spread sheet constitute the components within the aircraft. The weight is the weight of the component and the distance is the length from the propeller to the center of gravity of the component. The equation used to determine the center of gravity is

$$X_{c.g}=\frac{\sum_{i=1}^{i=13} X_{c.g.i}*W_i}{\sum_{i=1}^{i=13} W_i}$$

The bottom portion of the spread sheet is used to determine the travel of the center of gravity due to various passenger loadings.

CENTER OF GRAVITY TRAVEL					
ITEM	WEIGHT	DISTANCE	W*D		
speed control	3.23	4.94	15.9562		
motor	6.5	3.125	20.3125		
propeller	0.494	0			
battery (eng)	6.24	8.75	54.6		
battery (sys)	2	6.615	13.23		
reciever	0.95	7.59	7.2105		
servos	1.2	6.405	7.686		
nose casting	1.128	4.25	4.794		
landing gear	6	8	48		
	1	41	41		
structure					
body	11.8	20.7	244.26		
tail	5	48	240		
wing	10	17	170		
SUMMATION	55.542		867.0492		Xac=16
				C.G. LOCATION	15.6106946
PAYLOAD					
PASSENGERS	WEIGHT	DISTANCE	Wtot	(W*D)tot	C.G. LOC.
4	0.3527	19.7850	0.3527	6.9782	15.6370
8	0.3527	21.3550	0.7054	14.5101	15.6729
12	0.3527	22.9250	1.0581	22.5957	15.7181
16	0.3527	24.4950	1.4108	31.2351	15.7724
20	0.3527	26.0650	1.7635	40.4282	15.8358
24	0.3527	27.6350	2.1162	50.1751	15.9080
28	0.3527	29.2050	2.4689	60.4757	15.9888
32	0.3527	30.7750	2.8216	71.3300	16.0782
36	0.3527	32.3450	3.1743	82.7381	16.1759
40	0.3527	33.9150	3.5270	94.7000	16.2818
44	0.3527	35.4850	3.8797	107.2155	16.3958
48	0.3527	37.0550	4.2324	120.2848	16.5177
52	0.3527	38.6250	4.5851	133.9078	16.6474
56	0.3527	40.1950	4.9378	148.0846	16.7847
		total weight	60.4798		

Appendix C

These are the component contributions for the Cm_{cg} equation of section 5.1 :

Fuselage :

$$Cm_{o_f} = \frac{(k_2 - k_1)}{36.5\, S\, \bar{c}} \sum_{x=0}^{x=l_f} w_f^2\, (\alpha_{ow} + i_f)\, \Delta x$$

$$Cm_{\alpha_f} = \frac{1}{36.5\, S\, \bar{c}} \sum_{x=0}^{x=l_f} w_f^2 \frac{\partial \varepsilon_u}{\partial \alpha}\, \Delta x$$

Wing :

$$Cm_{o_W} = Cm_{ac_w} + C_{L_{ow}} \frac{(X_{cg} - X_{ac})}{\bar{c}}$$

$$Cm_{\alpha_W} = C_{L_{\alpha w}} \frac{(X_{cg} - X_{ac})}{\bar{c}}$$

Horizontal Tail :

$$Cm_{o_t} = \eta\, V_H\, C_{L_{\alpha t}}\, (\varepsilon_o + i_w - i_t)$$

$$Cm_{\alpha_t} = -\eta\, V_H\, C_{L_{\alpha t}} \left(1 - \frac{d\varepsilon}{d\alpha}\right)$$

where V_H is the horizontal tail volume ratio which is defined as

$$V_H = \frac{l_h\, S_h}{S\bar{c}}$$

The last component contribution, due to drag, is derived below using the definitions of the lift and drag coefficients for the wing.

$$Cm_D = C_{D_w} \frac{(Z_{ac} + Z_{cg})}{\bar{c}}$$

$$C_L = C_{L_{ow}} + C_{L_{\alpha w}}$$

$$C_{D_w} = C_{D_{ow}} + \frac{C_L^2}{(\pi\, AR\, e)}$$

These equations combine to form the drag contributions to Cm_o and Cm_α.

$$C_{m_{oD}} = C_{D_{0w}} \frac{(Z_{ac} - Z_{cg})}{\bar{c}}$$

$$Cm_{\alpha D} = \frac{1}{\pi\, AR\, e} (2\, C_{L_{ow}}\, C_{L_{\alpha w}} + C^2_{L_{\alpha w}}\, i_w) \frac{(Z_{ac} - Z_{ac})}{\bar{c}}$$

Appendix D

The following is a list of the variables and equations that were used to implement TKSolver Plus to analyze the stresses at the root of the wing due to lift and drag forces.

Input	Name	Output	Comment
.125	hc		spar cap height
.25	wc		spar cap width
.15	tc		%chord thickness
	t	1.8	thickness
	ar	7	aspect ratio
84	b		span
12	c		chord
	s	1008	wing area
1.5	n		load factor
1.5	fs		factor of safety
3.75	w		weight of a/c
.0058	db		density of balsa
.016	ds		density of spruce
.0625	ts		spar thickness
.0625	tr		rib thickness
.237	d		drag
16.2	arib		rib area
	wsc	.084	weight of spar cap
	ws	.0471975	weight of spar
	wle	.084	weight of leading edge
	wte	.168	weight of trailing edge
	wr	.0058725	weight of rib
	ww	8.19828	weight of wing
	izz	.04387858	z moment of area
	iyy	.00032552	y moment of area
	sxx	2772.7434	stress
	mz	88.59375	moment about z
	my	2.4885	moment about y
	sca	.03125	spar cap area

Equation

```
*       sca=hc*wc
*       ar=b^2/s
*       s=b*c
*       t=tc*c
*       wsc=2*hc*wc*b*ds
*       ws=(t-2*hc)*ts*b*db
*       wle=.25*.25*b*ds
*       wte=.5*.25*b*ds
*       wr=arib*tr*db
*       ww=(wsc+wle+wte+ws+22*wr)*16
*       izz=wc*hc^3/12+.5*hc*wc*(t-hc)^2
*       iyy=hc*wc^3/6
*       mz=.125*n*fs*w*b
*       my=.125*d*b
*       sxx=mz*t/2/izz+my*wc/2/iyy
```

Appendix E1: Take-off Spread Sheet

To evaluate the take-off performance of our aircraft, a spread sheet was developed which determined the time, velocity, and distance covered as the aircraft accelerated down the runway. These values were calculated for a small time increment. The calculations were performed until the lift equaled the weight of the aircraft, because at approximately this time, the aircraft will lift off the ground. For this method to be valid, it is assumed that the aircraft is held staionary by brakes until the motor and propeller reach steady rotation at the motor's maximum power setting. At this setting, the average thrust achieved is 1.3 lbs. The coefficeint of rolling friction for the runway was assumed to be 0.1, and the ground effect was minimized by taking the height of the wing to be it maximum height of 1.25 ft. These two assumptions are both probably high, and hence make the calculations a worst case scenario.

Equations used for Calculations:

$$L = 0.5 * r * V^2 * S * C_L$$

$$D = 0.5 * r * V^2 * S * \left(Cd,o + \frac{f * C_L^2}{p*e*AR} \right)$$

$$F = T - D - m\,(W - L)$$

$$\Delta V = \frac{F}{W/g} * \Delta t$$

$$V = V_{old} + \Delta V$$

$$\Delta S = V * \Delta t$$

$$S = S_{old} + \Delta S$$

$$t = t_{old} + \Delta t$$

The values used for each of the relevant parameters can be seen in the input section of the spread sheet.

TAKEOFF PERFORMANCE

Inputs

Weight (oz)	S (ft^2)	Rho	e	AR	Cl	Cdo	Wt (lbs)
58	7	0.00225	0.83	7	0.61	0.0288	3.625

wing ht (ft)	Thi	Fric Coeff	Prop	Thrust(lbs)	Vel initial	Delta t
1.25	0.8908686	0.1	Z10-6	1.3	0.05	0.1

Calculations

Time (s)	Xgr (ft)	Vel (ft/s)	L (lbs)	D (lbs)	F (lbs)	Delta V	V new	Delta S
0.00	0.00	0.05	0.000	0.000	0.938	0.833	0.883	0.088
0.10	0.09	0.88	0.004	0.000	0.938	0.833	1.716	0.172
0.20	0.26	1.72	0.014	0.001	0.938	0.833	2.549	0.255
0.30	0.51	2.55	0.031	0.002	0.938	0.833	3.382	0.338
0.40	0.85	3.38	0.055	0.004	0.939	0.834	4.216	0.422
0.50	1.27	4.22	0.085	0.007	0.939	0.835	5.050	0.505
0.60	1.78	5.05	0.123	0.009	0.940	0.835	5.886	0.589
0.70	2.37	5.89	0.166	0.013	0.941	0.836	6.722	0.672
0.80	3.04	6.72	0.217	0.017	0.942	0.837	7.559	0.756
0.90	3.80	7.56	0.274	0.021	0.944	0.838	8.397	0.840
1.00	4.64	8.40	0.339	0.026	0.945	0.840	9.237	0.924
1.10	5.56	9.24	0.410	0.032	0.947	0.841	10.078	1.008
1.20	6.57	10.08	0.488	0.038	0.949	0.843	10.921	1.092
1.30	7.66	10.92	0.573	0.044	0.951	0.844	11.765	1.177
1.40	8.84	11.77	0.665	0.051	0.953	0.846	12.612	1.261
1.50	10.10	12.61	0.764	0.059	0.955	0.848	13.460	1.346
1.60	11.44	13.46	0.870	0.067	0.958	0.851	14.311	1.431
1.70	12.87	14.31	0.984	0.076	0.960	0.853	15.164	1.516
1.80	14.39	15.16	1.105	0.085	0.963	0.855	16.019	1.602
1.90	15.99	16.02	1.233	0.095	0.966	0.858	16.877	1.688
2.00	17.68	16.88	1.368	0.105	0.969	0.861	17.738	1.774
2.10	19.45	17.74	1.511	0.116	0.972	0.864	18.601	1.860
2.20	21.31	18.60	1.662	0.128	0.976	0.867	19.468	1.947
2.30	23.26	19.47	1.821	0.140	0.979	0.870	20.338	2.034
2.40	25.29	20.34	1.987	0.153	0.983	0.873	21.211	2.121
2.50	27.42	21.21	2.161	0.166	0.987	0.877	22.088	2.209
2.60	29.62	22.09	2.344	0.180	0.991	0.881	22.969	2.297
2.70	31.92	22.97	2.534	0.195	0.996	0.885	23.854	2.385
2.80	34.31	23.85	2.733	0.210	1.000	0.889	24.742	2.474
2.90	36.78	24.74	2.941	0.226	1.005	0.893	25.635	2.564
3.00	39.34	25.64	3.157	0.243	1.010	0.897	26.532	2.653
3.10	42.00	26.53	3.382	0.260	1.015	0.902	27.434	2.743
3.20	44.74	27.43	3.615	0.278	1.021	0.907	28.341	2.834

Appendix E2: Take-off Performance Variation with Ground Effects

In order to determine the variation of take-off performance due to ground effects, a fortran program was developed. Ground effects were investigated by varying the height of the wing from the ground. The results from the program (See Figure E2-1) indicate that the difference in take-off distance from various wing heights is negligible.

Figure E2-1
Take-off Distance vs. Alpha for Various Heights of the Wing

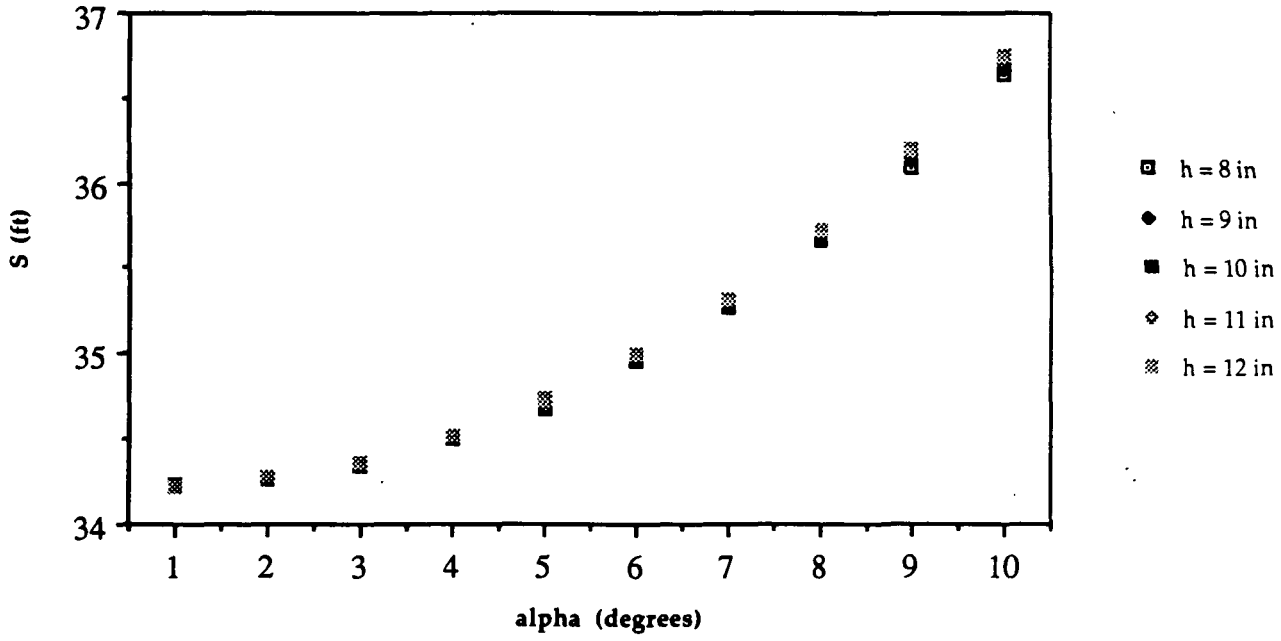

Fortran Program to Determine Variation in Take-off Distance

```
c       Take-off Distance
c
        real l
        dimension s(5.10), v(5,10)
        dt=.001
        delv=0
        vn=0
        dels=0
c
c
        do 4 k=1,5
        h=k+7
        phi=(5*h/7)**2/(1+(5*h/7)**2)
c
        do 3 m=1,10
        alpha=m
        v(k,m)=0
        s(k,m)=0
c
        cl=.079*(alpha+4)
        do 1 n=0,100000
        l=.5*.00225*v(k,m)*v(k,m)*7*cl
        d=.5*.00225*v(k,m)*v(k,m)*7*(.014+phi*cl*cl/(3.1417*.84*7))
c
        delv=32.2*(0.267-d/3.75-.04*(1-1/3.75))*dt
        vn=v(k,m)+delv
        dels=.5*(v(k,m)+vn)*dt
        s(k,m)=s(k,m)+dels
        v(k,m)=vn
        if(v(k,m).ge.22.2)then
              goto 2
        endif
 1      continue
c
c       output
c
 2      open(unit=121,status='unknown',file='out')
        write(121,*) v(k,m),char(9),s(k,m)
 3      continue
 4      continue
        stop
        end
```

Appendix E3: Turning Performance

To predict the turning performance of the Initial Guess, the following spread sheet was developed. This spread sheet calculates the turn radius, turn rate, and bank angle of a steady, level, banked turn for a range of C_L's using the estimated weight of 60. The lift for a range of C_L's is used to calculate the load factor. This load factor along with velocity and the acceleration due to gravity may then be used to calculate the turn radius, turn rate, and bank angle. These calculations were done at a range of velocities in order to determine what cruise speed was necessary for a maximum turn radius of 60 ft or less. The required lift necessary to make a steady, level, banked turn is provided with a cruise velocity of 28 ft/s.

Equations used for calculations:

Lift: $$L = C_L * \frac{1}{2} * r * V_{cruise}^2 * S$$

Load Factor: $$n = \frac{L}{W}$$

Turn Radius: $$R = \frac{V_{cruise}^2}{g \sqrt{n^2 - 1}}$$

Turn Rate: $$w = \frac{g \sqrt{n^2 - 1}}{V}$$

Bank Angle: $$f = \frac{180}{p}$$

AT V = 28 FT/S						
WEIGHT (LB)	CL	LIFT	LOAD FACTOR	TURN RADIUS (FT)	TURN RATE (1/S)	BANK ANGLE (DEG)
3.6	0.60	3.704	1.029	100.3738	0.279	13.635
	0.65	4.013	1.115	49.4259	0.567	26.225
	0.70	4.322	1.201	36.6558	0.764	33.592
	0.74	4.569	1.269	31.1585	0.899	38.003
	0.75	4.630	1.286	30.0972	0.930	38.971
	0.80	4.939	1.372	25.9198	1.080	43.207
	0.85	5.248	1.458	22.9550	1.220	46.685
	0.90	5.557	1.544	20.7083	1.352	49.616
	0.95	5.865	1.629	18.9292	1.479	52.135
	1.00	6.174	1.715	17.4752	1.602	54.330
	1.05	6.483	1.801	16.2583	1.722	56.265

REFERENCES

1. ---, A Catalog for Low Reynolds Number Airfoil Data for Wind Turbine Applications, U.S. Department of Commerce, National Technical Information Service.

2. Anderson, John D., Introduction to Flight, McGraw-Hill Book Company, New York, 1985.

3. Asson, Kenneth M., Master Thesis, "The Development of an Advanced Dynamometer System to Experimentally Determine Propeller Performance," U. of Notre Dame Department of Aerospace Engineering, April 1990, pp. 66, 69.

4. Beron-Rawdon, Blaine, Model Aviation, "Dihedral," four part series, August, September, October, and December 1989.

5. Dunn, Patrick F., AE 454 - Lecture No. 18, "Electric Motor - Propeller Propulsion," University of Notre Dame, Nov. 1, 1990.

6. Jenson, Daniel, Master Thesis, "Subsonic Drag Determination," University of Notre Dame, 1988.

7. Lennon, A.G., R/C Model Airplane Design, Osceola, WI, Motorbooks International Publishers and Wholesalers, Inc., 1989.

8. Nelson, Dr. Robert C., Flight Stability and Automatic Control, New York: McGraw-Hill Book Company, 1989.

9. Nelson, Dr. Robert C., AE 441 - Lecture Notes, "Subsonic Drag Breakdown Method," University of Notre Dame, Feb. 5, 1991.